NASA TECHNICAL NOTE

NASA TN D-2938

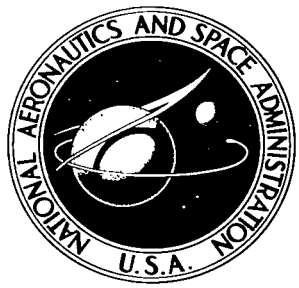

NASA TN D-2938

A WIDE-RANGE PIEZOELECTRIC MOMENTUM TRANSDUCER FOR MEASURING MICROMETEOROID IMPACTS

by Vernon L. Rogallo and Frank Neuman

Ames Research Center
Moffett Field, Calif.

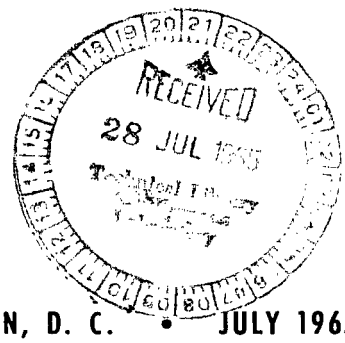

NATIONAL AERONAUTICS AND SPACE ADMINISTRATION • WASHINGTON, D. C. • JULY 1965

A WIDE-RANGE PIEZOELECTRIC MOMENTUM TRANSDUCER FOR MEASURING MICROMETEOROID IMPACTS

By Vernon L. Rogallo and Frank Neuman

Ames Research Center
Moffett Field, Calif.

NATIONAL AERONAUTICS AND SPACE ADMINISTRATION

For sale by the Clearinghouse for Federal Scientific and Technical Information
Springfield, Virginia 22151 – Price $3.00

TABLE OF CONTENTS

A WIDE-RANGE PIEZOELECTRIC MOMENTUM TRANSDUCER FOR MEASURING MICROMETEOROID IMPACTS

By Vernon L. Rogallo and Frank Neuman
Ames Research Center

SUMMARY

A new piezoelectric momentum transducer has been developed and tested in the laboratory with low-velocity particles and with simulated micrometeoroids at hypervelocities.

The transducer is a simple design incorporating two piezoelectric ceramic beams which serve both as the sensor and as leaf springs. The beams are arranged to support a target in such a manner as to restrict motion primarily to one direction. Although the transducer is very sensitive, capable of momentum measurements of the order of 10^{-5} dyne-sec, it is rugged, being able to withstand high g loads. It can be operated at any altitude with equal sensitivity.

When the momentum transducer is used as an impulse detector, the output is directly proportional to the component of impact transferred to the target in a direction parallel to the transducer principal axis. Its sensitivity is essentially independent of the location of impact on the target area. The transducer and associated electronics can be calibrated at various momentum levels by a remote process.

The unique characteristics of the transducer make it a valuable laboratory device. At the Ames Research Center it has had the following applications: a narrow band-pass electromechanical filter, an ultrasensitive vibration pickup, a laser energy calibrator and impact transducer, a force transducer for measurement of ion-beam accommodation factor, and a ballistocardiograph for the measurement of motion of small living organisms or components such as heart beat reactions.

INTRODUCTION

The most sensitive micrometeoroid transducers flown to date have incorporated a piezoelectric sensing element. Such a transducer is referred to as a microphone detector, and measurements made by the device represent the first substantial direct measurement of interplanetary matter in the vicinity of the earth. The response characteristics of the microphone detector have been the subject of considerable debate. An impacting micrometeoroid generates in the detector target a transient mechanical pulse which is subsequently transformed into an electrical signal by a piezoelectric crystal. The transformation is complex and it is not certain precisely what is being measured. The usefulness of the detector, aside from detecting number of impacts, is directly

dependent on laboratory momentum calibration techniques. One feature inherent in the detector design results in a response which is a function of impact position on the target. The momentum threshold sensitivity of a typical microphone detector (for the Explorer I satellite) has been reported to be of the order of 10^{-3} dyne-sec (ref. 1).

In view of the state of the art, an attempt was made to develop a new device which would provide detection and a quantitative impact momentum measurement at a threshold of the order of 10^{-5} dyne-sec. Also consideration was given to additional features such as uniform sensitivity over the target area and means for in-flight calibrations.

As an outgrowth of this study a new piezoelectric momentum transducer has been developed and tested in the laboratory with low-velocity particles and with simulated micrometeoroids at hypervelocities. The device is unique and its characteristics make it applicable to a wide variety of uses.

Presented herein is a complete description of the transducer, its operation, design details, and calibration techniques. In addition, there are included pertinent details of an integral absolute calibrator and an arrangement for the rejection of mechanical common-mode noise. Typical test results are presented to show the transducer response to low and hypervelocity impacts, both normal and oblique to the target, and at different relative positions on the target area. Since the usable threshold of the transducer is dictated by the signal-to-noise ratio, a section on mechanical and electrical noise is included.

In order to show the versatility of the transducer, several quite diversified applications to various research fields at the Ames Research Center are presented.

SYMBOLS

A	area of the capacitor plates, m^2
B	bandwidth, cps
B_o	rms bandwidth, cps
B_v	rms bandwidth of the detected and summed noise voltages, cps
C_d	damping coefficient, kg/sec
C_e	transducer electrical capacitance, F
C_m	mechanical compliance, m/newton
C_l	load capacitance, F
d	maximum displacement of the mass, m

E	output voltage of the unloaded transducer, V
E_o	output energy, J
F	static force, newtons
f_n	undamped natural frequency, cps
$f(t)$	driving function (force), newtons
I	current, A
I_b	plane area moment of inertia, m^4
i	imaginary component of a number
K	spring constant, newtons/m
K.E.	kinetic energy, J
k	Boltzmann's constant, J/molecule - ^oK
k_p	momentum transfer parameter of proportionality
L	beam span, m
M	total mass, kg
M_a	maximum bending moment, newton-m
M_b	maximum bending moment, newton-m
m	projectile mass, kg
m_b	equivalent beam mass, kg
m_s	stem mass, kg
m_V	mean of $p(V)$
N	electromechanical linear transducer ratio, V/newton
NF	noise figure
N_p	momentum transducer ratio, V/newton-sec
$\overline{N(V_o)}$	mean number of threshold crossings of the level V_o/sec due to noise
n	noise power, W

P	applied load, newtons
P.E.	potential energy, J
p_i	projectile momentum, newton-sec (1 newton-sec = 10^5 dyne-sec)
$p(V_o)$	probability density function of V_o
p_x	target momentum in the direction of the principal axis, dyne-sec
$p[x(t)]$	probability density function of $x(t)$
Q	B_f/B_t bandwidth ratio
q	charge, coulombs
R	resistance, ohms
S	separation of the capacitor plates, m
$S_x(f)$	power spectral density of the transducer
T	absolute temperature, ^oK
t	time, sec
t_m	length of time force is applied, sec
$t(0+)$	time of impact, sec
$u(t)$	unit step function starting at time 0
$u(t - \tau)$	unit step function starting at time τ
V	voltage, V
$\hat{V}$	peak output voltage, V
V_i	initial target velocity, m/sec
V_o	threshold voltage, V
$V(t)$	envelope of the narrow band random process
v	dummy variable of integration
W	output power, W
x	deflection, m
$\dot{x}$	velocity, m/sec

$\ddot{x}$	acceleration, m/sec^2
x_o	maximum deflection, m
$x(t)$	gaussian noise voltage, V
$x(\omega)$	system function
x_1	maximum amplitude of the deflection envelope, m
Y	modulus of elasticity, $newtons/m^2$
$y(t)$	noise voltage of the random process, V
α	damping constant, 1/sec
Δ	interval or change of a quantity
$\delta(t)$	impulse function
ϵ_o	permittivity, F/m
τ	time duration of a rectangular impulse, sec
σ^2	mean square noise voltage of $x(t)$, V^2
σ_{ideal}^2	minimum noise power, V^2
σ_v^2	variance of $p(v)$, V^2
φ	phase delay between forcing function and deflection, radians
ω	radian frequency, 1/sec
ω_{max}	frequency of maximum response for forced vibrations, 1/sec
ω_n	undamped natural frequency, 1/sec
ω_o	damped natural frequency, 1/sec

DESCRIPTION OF MOMENTUM TRANSDUCER

Basic Transducer Components

Basically, the transducer consists of a simple spring-mass system wherein a target is suspended so that its motion is restricted primarily to one direction. The essential components of the momentum transducer are shown in figure 1(a). The target and stem form an integral mass rigidly attached to two widely spaced parallel piezoelectric ceramic beams. The beams, at the opposite ends, are attached to a common support. These beams serve not only as

the springs of the suspension but also, by their inherent piezoelectric characteristics (mechanical to electrical energy converters), as motion sensing elements. Further, the beams are appropriately oriented to be sensitive in terms of voltage output relative to motion in the direction of the principal axis of the transducer. Silver electrode material is bonded to the surfaces of maximum stress. The beams are inserted through the stem and support and are bonded in place with a nonconductive epoxy cement. The silver electrode material in this area is removed prior to bonding to improve mechanical end fixity and electrical insulation. The silver electrode material is also removed in the center portion for electrical reasons which are discussed in appendix A.

For ruggedness, a stop member is attached to the support (fig. 1(a)). This member is provided with an oversize bore (fig. 1(b)) to receive the stem so as not to interfere with vertical motion but to provide lateral limits and/or torsional limits about a transverse axis. In addition, the stop member is provided with passages which are coaxial to those through the stem (fig. 1(c)). Two pins are inserted through the horizontal passages. The locking pin fits snugly in the stop member as well as in the stem and when the transducer is not in use, helps to prevent damage due to shock loads caused by rough handling, transportation, etc. In contrast, the overload stop pin is snugly received in the stop member but is received in an oversized passage in the stem. This arrangement provides an overload limit in the direction of the principal axis of the transducer. Metal shields protect the ceramic beams and associated electrical leads against damage. The shields serve a twofold purpose in also providing electrical isolation from stray fields. A prototype transducer with shielding removed is shown in figure 2(a). An assembled transducer with preamplifier attached is shown in figure 2(b).

Sensing Elements

The piezoelectric beams used as sensing elements in all transducers discussed herein are a polycrystalline modified lead zirconate titanate ceramic. Its high curie temperature, about 300° C, makes it an ideal sensing element over a wide temperature range. The ceramic has a high dielectric constant, 1600, which minimizes cable loading effects on its performance. The beam dimensions and equivalent circuit for a cantilever beam are summarized in table I.

The beam is a single element with a series of parallel holes, running the length of the element, coated with graphite to provide the central conductor required for polarization. The flat surfaces of the beam parallel to the plane of the hole pattern are coated with silver. These electrodes form the electrical capacitance across which the charge is developed. The charge developed is proportional to the beam deformation.

Integral Absolute Calibrator

The transducer can be simply modified, if desired, to incorporate an absolute calibration unit in the form of a pair of electrostatic plates. (See fig. 3.) The movable plate is an aluminized quartz disk attached to the lower end of the stem. The stationary plate and guard ring are mounted on a dielectric-support fixture attached to the transducer support. The aluminized quartz disk is electrically insulated from the stem and a fine wire is attached between the disk and the guard ring. The electrostatic components are enclosed by metal plates and the outside of the dielectric-support fixture is coated with a conductive type paint. Thus the electrostatic unit is electrically shielded from the transducer and surroundings. The components are shown in figure 3(b) and an assembled transducer is shown in figure 3(c).

Mechanical Common-Mode-Noise Rejection

A transducer which is capable of detecting very minute impacts is inherently a sensitive accelerometer and hence responds to any accelerations induced through its mounting. In order to suppress unwanted electrical signals mechanically induced through mounting supports, a compensator was added, amounting essentially to a second transducer mounted on the same support member. (See fig. 4.) The second transducer is made identical with the exception that a dummy volume of equal mass is used in place of the target. The two transducers are arranged so that their principal axes are parallel and are located as close together as a side-by-side arrangement will allow with the transducers inverted with respect to each other. Thus, any extraneous vibrations will be equally detected by both the primary and secondary unit, and the electrical output from the secondary unit can be subtracted from the output of the primary unit to attenuate all responses except those caused by impacts on the target of the primary unit.

THEORY OF OPERATION

The design of the momentum transducer provides an instrument which will respond to either steady-state or transient inputs. These inputs can be induced mechanically or electrically. This feature makes the transducer applicable to a wide variety of uses and to unique calibration techniques. Since the transducer was primarily designed for measuring impacts of micrometeoroids, the discussion herein will be devoted to response relations associated with transient inputs.

Transducer Momentum Response

The principal aspects of the response of the transducer to an impact are amenable to a very simple analysis if the duration of the impact is short compared to the natural period of the transducer, the system is lightly damped, the mass of the impacting particle is much less than the mass of the target, and the support has infinite mass.

Under these conditions an impact will transfer momentum to the target mass according to the equation

$$p_x = k_p p_i \tag{1}$$

where

p_i projectile momentum

p_x target momentum

k_p momentum transfer parameter of proportionality; 1 for completely inelastic impact and 2 for completely elastic impact

The value of k_p may lie anywhere between 1 and 2 and, in the case of impacts which produce ejecta from the target, k_p may exceed 2. From the definition of momentum,

$$p_x = MV_i \tag{2}$$

where

M target mass (including stem and effective beam mass)

V_i target velocity

The impact imparts a kinetic energy to the system

$$\text{K.E.} = \frac{1}{2} MV_i^2 \tag{3}$$

If V_i is substituted from equation (2)

$$\text{K.E.} = \frac{p_x^2}{2M} \tag{4}$$

If one assumes no internal loss in the system, then at the peak of the deflection the kinetic energy is converted to potential energy

$$\text{K.E.} = \text{P.E.} = \frac{1}{2} Kx_o^2 \tag{5}$$

where

K spring constant

x_o maximum displacement of the mass

Combining (4) and (5) and solving for x_o, we have

$$x_o = \frac{p_x}{\sqrt{KM}} \tag{6}$$

From equation (6) it can be seen that the peak spring deflection is directly proportional to the target momentum. Following the peak deflection the system will oscillate in a decaying sinusoidal transient.

If the projectile momentum is desired, the momentum transfer constant, k_p, must be considered. The relationship of target displacement in terms of projectile momentum can be expressed as follows:

$$x_o = \frac{k_p}{\sqrt{KM}} p_i \tag{7}$$

In order to meet the assumed condition that the duration of the impact, t_m, is short compared with the period of the transducer, the condition should be satisfied that

$$t_m \ll \frac{1}{f_n}$$

where f_n, the natural frequency of an undamped spring-mass system, is well known to be

$$f_n = \frac{1}{2\pi}\sqrt{\frac{K}{M}} \tag{8}$$

Transducer Response to Various Types of Drive Force

The complete equation of motion for the transducer is

$$M\ddot{x} + C_d\dot{x} + Kx = f(t) \tag{9}$$

The solutions for various types of driving forces are given in table II. The responses resulting from the diversity of driving forces suggest calibration procedures as well as many applications of the transducer, in addition to the measurement of momentum of micrometeoroids.

The complete equation for the response to an impulse is given in row IV of table II. It confirms the simplified analysis that for an impulse the maximum amplitude of the envelope of the decaying exponential is directly proportional to the input momentum.

For various applications associated with impacts and calibration techniques, it is of interest to determine the effect of impact duration on the transducer response. For this purpose it is logical to determine response characteristics for rectangular pulses of driving force of various durations but with their amplitudes inversely proportional to their duration so that the

momentum is the same in each case. The transducer with integral calibrator lends itself to this simple drive force input. The differential equation is

$$M\ddot{x} + C_d\dot{x} + Kx = \frac{p_x}{\tau}\,[u(t) - u(t - \tau)] \tag{10}$$

Since for the transducer $\omega_o \approx \omega_n$, the simplified solution results in a response for $t > \tau$ as shown in row V of table II. The calculated response of the transducer (the variation of the maximum amplitude of the envelope of the decaying exponential) with time duration is shown in figure 5. It may be noted that the time duration of the pulse can have an appreciable influence on the transducer response. However, even when the pulse duration is as great as one fourth of a cycle of the resonant frequency of the transducer the response is still 88 percent of that corresponding to a true impulse input. It is anticipated that input pulses having shapes other than rectangular would produce quite similar responses.

TRANSDUCER DESIGN CONSIDERATIONS

Mechanical Compliance and Resonant Frequency

The piezoelectric beams of the transducer are in the form of fixed-end beams with one end displaced by the motion of the target. (See fig. 6.) The free-body diagram is shown in figure 6(b) where P is the force applied to the beam. From consideration of symmetry, and the fact that the center point is a point of inflection ($M_o = 0$), it is apparent that each half of the beam behaves as a cantilever beam as indicated in figure 6(c). The over-all deflection of the beam is twice that of one of the cantilevers, that is,

$$x = \frac{2P(L/2)^3}{3YI_b} \tag{11}$$

Since there are two beams supporting the target, $P = F/2$ if the force on the target is F, and

$$x = \frac{F(L/2)^3}{3YI_b} \tag{12}$$

This is precisely the same deflection as for a cantilever beam of length $L/2$ and applied force F. One may therefore compute the mechanical compliance ($C_m = 1/K$) directly from the formula for C_m' in table I, using the above values for length and force.

For a precise computation of the natural frequency, allowance must be made for the effective mass of the beams since the elements at different points along the beams enter to varying extents into the motion. The resonant frequency of an undamped cantilever beam with a concentrated mass at the end has been computed by the energy method in reference 2 and the effective

mass of the beam proper was found to be 0.236 times the real mass. Performing the equivalent computations for one beam of the momentum transducer results in a factor of 0.309, that is, greater by a factor of 1.31, so that the natural frequency is, in terms of the simple cantilever beam equivalent mass (m_b'),

$$\omega_n = \sqrt{\frac{1}{[M + 1.31(2m_b')]C_m}} \tag{13}$$

where the factor of 2 accounts for the presence of the two beams of the transducer.

Although the influence of damping on the resonant frequency may not be significant for some applications, the damping is of considerable significance for the performance of the transducer in terms of the decay time. Unfortunately the damping cannot be precisely determined in advance because of lack of knowledge of the beam material and because of indeterminates associated with the beam-end fixity. However, the damping is readily obtained experimentally from measurement of the decay rate of the free vibration and can usually be tailored to suit the application.

Transducer Voltage Output

Since the charge generated in any portion of a beam is proportional to the area under the moment diagram, the over-all voltage between the full upper and lower surfaces of one of the beams would be zero because of the opposite direction of the bend in the two halves. For this reason a gap is made in the electrodes at midspan and the two halves are connected in parallel. (Note appendix A.) Only one beam is used for the output signal; the other beam is reserved for calibration purposes. With this arrangement the voltage output is that of one-half beam, and the capacitance is twice that of one-half beam. For the typical cantilever of table I with force P, the output voltage E' is

$$E' = N'P = 0.56 \frac{L'}{wt} P, \text{ volts} \tag{14}$$

For the actual cantilever half-beam $L' = L/2$ and $P = F/2$ so that

$$E = 0.56 \frac{L/2}{wt} \left(\frac{F}{2}\right) \tag{15}$$

and

$$N = \frac{E}{F} = 0.14 \frac{L}{wt} \tag{16}$$

In these equations the primed symbols refer to the typical cantilever equations; whereas the symbols without primes refer to the actual transducer and the total target force F.

Similarly,

$$C_e = 2(450)\frac{(L/2)w}{t} = 450\frac{Lw}{t}\ ,\ \mu\mu f \tag{17}$$

(Note that in eqs. (14) through (17), L, w, and t are in inches.)

For the application of the transducer to the measurement of impacts it is of interest to relate the transducer voltage response to the input momentum. From equation (6) for the peak deflection due to an impact, the corresponding maximum force is

$$F = Kx_o = \frac{Kp_x}{\sqrt{KM}} = p_x\omega_n \tag{18}$$

with a corresponding output voltage

$$E = N \cdot F = Np_x\omega_n \tag{19}$$

Defining the momentum transducer ratio as $N_p \equiv E/p_x$, then one obtains

$$N_p = \omega_n N \tag{20}$$

MEASUREMENTS AND TEST RESULTS

Calibration Techniques

Low-velocity impacts.- Many techniques have been devised (ref. 3) for calibrating microphone detector systems with small particles traveling at relatively low velocities. The generally accepted technique involves the dropping of spherical beads of various sizes and densities from a known height. This technique has many limitations and is impractical for momenta below 10^{-3} dyne-sec. However, as an expedient technique for obtaining momenta of this value and higher, the bead-drop technique was employed. In order to assure consistent values of momentum for consecutive drops, a bead release technique different from that of reference 3 was devised. This consisted in using a very finely drawn glass tube in which the internal pressure could be reduced sufficiently to hold a bead in contact with the glass at the fine drawn end, thereby assuring a consistent drop height. To provide a consistent release of the bead, the pumping source was inactivated and the bead would fall free at the instant when the weight of the bead had exceeded the equivalent force produced by the slowly increasing internal pressure. The beads were dropped on a very thin layer of modeling clay on the target so that they would come to rest upon impact; thus rebounding was eliminated.[1]

[1]In the case of a bead drop the input includes, in addition to the desired impulse force produced by the bead on impact, a step force produced by the weight of the bead. The step function produces a constant displacement superimposed on a damped cosine wave (see table II, row II). The constant displacement is not seen by the ac-coupled instrumentation and the damped cosine wave is 90° out of phase with the impulse response. (See table II, row IV.) Thus the effect of the damped cosine wave when combined with the sine wave response is less than 5 percent for the lowest drop height used (3 cm).

Controlled induced displacement.- Although the bead-drop technique substantiated that the transducer is linear over a range from 10^{-3} to 1 dyne-sec, as was anticipated by theory, it was desirable to determine the usable threshold of the transducer as limited by the signal-to-noise ratio. A convenient means for applying precisely controlled calibrating forces covering the entire transducer range is available in the piezoelectric beams. If a voltage is applied to one of the piezoelectric beams, a charge results which distorts the beam, deflecting the target. With a dc voltage this displacement remains fixed as long as the potential is applied. However, when the switch is opened and the beam charge allowed to dissipate suddenly through a shunt resistor, the suspended mass will vibrate freely. The response obtained by this technique is almost indistinguishable from that obtained by a true impact on the target. A typical momentum calibration curve is shown in figure 7. These data were obtained by both the bead-drop and induced-deflection techniques. It may be noted that the transducer response is directly proportional to impact momentum. The repeatability obtained by the induced-deflection technique was excellent to an equivalent momentum of the order of 10^{-5} dyne-sec, at which level the signal began to be lost in noise. The voltage for the deflection technique was reduced in steps to the order of a few millivolts in order to simulate impacts of less than 10^{-5} dyne-sec. To obtain a favorable signal-to-noise ratio so that the low momentum threshold could be determined, the transducer was suspended by rubber bands in a chamber which was then evacuated.

Integral absolute calibrator.- The integral absolute calibrator, as previously discussed and shown in figure 3, can be used in lieu of the beam-induced displacement technique to produce essentially identical results. The advantage of the technique is that the calibrator, being absolute, requires no reference and further, is independent of any changes in the transducer characteristic which might conceivably be brought about, for example, by environmental conditions. The calibrator does, however, require additional hardware. The movable disk adds mass to the target and higher calibration voltages are required. A significant feature of the absolute calibrator is that a pulse of known force and duration can be directly induced through the stem of the transducer. For simulating impacts, the pulse duration must be short compared to the transducer's natural period of oscillation, as has been previously discussed in the theory of operation.

The equations applicable to the calibrator are as follows:

$$p_x = \int_o^{t_m} f(t)dt = Ft_m \qquad \begin{array}{c} \overline{\uparrow V \downarrow} \\ \rightarrow |t_m| \leftarrow \end{array} \qquad t_m \ll \frac{1}{f_n} \tag{21}$$

The force determined by the capacitor geometry and applied voltage (ref. 4) may be written as:

$$F = \frac{1}{2} \epsilon_o \frac{A}{S^2} V^2 \tag{22}$$

where ϵ_o is the dielectric constant of the air in the gap, S is the spacing between the plates, and A is the effective plate area. The momentum equation may thus be rewritten as:

$$p_x = 4.43 \times 10^{-12} \frac{A}{S^2} V^2 t_m, \text{ newton-sec} \qquad (23)$$

The capacitor voltages are quite high compared to the output voltage of the transducer; hence adequate electrical shielding is essential so that the capacitor voltage will not induce voltage in the piezoelectric beams or leads. Having established that the instrument output is linear with momentum, one can then make a simple test to determine the presence or absence of interference by reviewing a plot of transducer output as a function of the square of the capacitor input voltage. A linear variation indicates the absence of interference.

Response Relative to Impact Location

One of the basic requirements in the design was that the detector target have uniform sensitivity over its entire area. Tests employing the bead-drop technique were made to evaluate this feature. Typical results of the tests are shown in figure 8. These data were obtained by impacts of nearly constant momentum along the axis of a 10-cm rigid target at various distances from the principal axis of the transducer. The variation is considered small, particularly in contrast with microphone-type transducers (ref. 5). It should be pointed out that the variation can be considerably reduced, if desired, by increasing the beam spacing and/or reducing the beam length.

Response Relative to Angle of Impact

After it was ascertained that the transducer response was directly proportional to momentum in a direction parallel to the principal axis of the transducer, it was then of interest to determine the transducer response resulting from the impact of a particle having momentum in a direction oblique to the transducer principal axis. Since hypervelocity impact phenomena are not clearly understood and there is a dearth of information as to momentum or energy transfer at oblique angles, the tests of directional response were made by the low-velocity bead-drop technique. Moreover, as shown in the sketches (fig. 9), the target surface was maintained in a horizontal plane for each angle tested in order to assure that an axial component of momentum proportional to $\cos \theta$ and a transverse component proportional to $\sin \theta$ are applied to the stem of the transducer. The data are presented in figure 9 superimposed on a cosine curve to show any deviation from a true single-degree-of-freedom response. Good agreement is shown for low-speed impacts.

Response to Hypervelocity Particle Impacts

In order to simulate micrometeoroid impacts, a modified 2-million volt electrostatic accelerator was used. The facility and its operation are described in reference 6. Instrumentation similar to that used in the test to measure velocity and particle mass is discussed in reference 7. The accelerator and associated instrumentation were made available by contract with the

Space Technology Laboratory, Redondo Beach, California. The tests were made at their laboratory with the assistance of the Physical Research Division staff. A photograph of the test setup is shown in figure 10. The base of the Van de Graaff accelerator can be seen through the opening in the wall at the right. The launching tube extends from there to the micrometeoroid transducer chamber at the end to the left. The two boxes along the tube house velocity and particle alinement detectors. An additional alinement detector having a 3/16-inch opening is located at the end of the tube adjacent to the transducer target. The entire enclosure is evacuated to a pressure of the order of 10^{-5} torr. A schematic diagram of the apparatus and instrumentation is shown in figure 11.

The impact momentum as measured by the transducer is shown as a function of particle momentum in figure 12 for several target materials. The accelerated particles were iron spheres for all tests. The particle diameters ranged from 1.6 to 4.5 microns for a velocity range of 4 to 1.3 km per second, respectively. The accuracy of measurement of the velocity was believed to be approximately 1 percent and of the mass, 10 percent. Although the target materials were greatly different in composition (stone, plastic, and metal) the momentum transfer constant of proportionality is shown to be between 1 and 2. The major portion of the data was obtained for momenta from 10^{-5} to 10^{-4} dyne-sec. The upper limit was set by the capability of the accelerator and the lower by the environmentally induced mechanical noise. The tests were made under adverse noise conditions. The signal-to-noise voltage ratio for the 67 impacts shown in figure 12 had a mean value of 5.0 with a standard deviation of 2.5. The subject of noise, both electrical and mechanical, and isolation techniques will be discussed subsequently.

MECHANICAL AND ELECTRICAL NOISE

Noise Suppression Techniques

The transducer and the associated electronic system are subject to both mechanical and electrical noise. Mechanical noise is particularly troublesome because of the extreme sensitivity of the transducer and the difficulty of avoiding small shocks and vibrations in the environment. In its use in the laboratory, the minimum threshold (maximum sensitivity) of the transducer for quantitative measurements has been dictated predominately by the mechanical noise. For this reason the minimization of mechanical noise will be considered first. A more detailed analysis of the noise problem is given subsequently, including consideration of a detection scheme which would be applicable for a micrometeoroid detector where the impact rate is low.

Isolation from mechanical noise.- The design frequency of the transducer (approximately 140 cps), which was selected from a consideration of electrical noise interference in the laboratory, is in a region which is known to be difficult to isolate mechanically. It was found during the development of the transducer that the most expedient and efficient isolation was obtained by suspending the transducer by common gum-rubber bands.

For the hypervelocity impact tests (see measurements and tests results) where physical particles were used, this technique was not considered feasible since precise location and angle of the impact was desired. Since the particles were accelerated in a horizontal plane (fig. 10) and the transducer principal axis was also in a horizontal plane, a compound pendulum suspension having a low natural frequency was employed (fig. 13). The transducer base rested on a 4-pound lead mass which was in turn supported by four shock mounts attached to a cradle. The cradle was suspended by two wires with its center of gravity slightly below the fulcrum, or hinge point. The vacuum chamber (fig. 10) was supported by commercial shock mounts and the system tuned to a very low frequency by adding mass. To further complicate the problem, a heavy belt-driven drum unit in the Van de Graaff generator induced severe vibration along the launch tube. This was essentially eliminated by constructing the launch tube of several sections which were independently supported but interconnected by rubber tubing. An air bearing was used between the shock-mounted chamber and the support platform so that the chamber could essentially float in the longitudinal direction of the launch tube. In order to maintain a balanced system when the chamber-launch-tube assembly was evacuated, a bungee cord was attached on the opposite side of the chamber, alined in the direction of the axis of the launch tube, and directed over a pulley to a dead weight near the floor. The system was sufficiently effective to allow impact measurements at a threshold of the order of 10^{-5} dyne-sec, as shown in figure 12. The results were even more impressive when one considers that heavy machinery was being operated in adjacent rooms in addition to refrigerators, blowers, mechanical vacuum pumps, etc., in the test room. In addition, one side of the laboratory, adjacent to commercial roads, was solid glass; and heavy vehicular traffic of all types was prevalent during the entire test.

Mechanical common-mode-noise rejection.- In order to eliminate complex shock-mounting systems which are bulky and may involve heavy masses, it is most desirable to devise a system for noise suppression which is compact and light in weight, and which can be made integral with the transducer. Such a system was designed in the form of an essentially duplicate compensating transducer as previously described in the general description of the momentum transducer. Although a very limited amount of time was expended on the common-mode-noise-rejection feature, the test results were impressive. In order to determine the effectiveness of this feature, wide-band gaussian noise was introduced in the direction of the principal axis of the transducer at its base by means of a shaker driven by a noise generator. Typical results are shown in figure 14 where comparative outputs are shown for the target unit with the dummy made inoperative by a mechanical lock and with the common-mode-noise-rejection feature operable. The responses shown in figure 14(a) were obtained for identical impacts. It may be noted that the results are essentially the same. Figure 14(b) shows the responses due to wide-band gaussian noise input. The effectiveness of the noise rejection by the common-mode-rejection transducer is appreciable. The results shown in figure 14(c) illustrate the effectiveness of the common-mode-noise-rejection feature in measuring an impact in the presence of noise. Prior to making the test, the target and dummy units were tuned to 140 cps with an accuracy of 0.2 cps relative to each other by simply adding mass to the unit having the higher frequency. The outputs of the target and dummy units were amplified independently and viewed simultaneously by use of an oscilloscope. The outputs of the

units were sinusoidal but differed in amplitude and phase. Obviously the phase difference precluded attaining a null by adjusting the gains to equal output voltages and then subtracting outputs. Hence the gains were adjusted to obtain a minimum voltage when subtracted. The remaining voltage was 10 db below the output voltage of the target unit alone.

It is apparent that the two units were not a perfect match. Perhaps a better response match could have been obtained by changing the electrical load impedance of the lower beam of the lower frequency unit, to induce an equivalent compliance change, rather than by adding mass to the higher frequency unit. When the transducer with common-mode-noise-rejection feature was mechanically excited at precisely its resonant frequency, a 50 db rejection (400/1 signal-to-noise ratio) was realized. This becomes very significant for applications where narrow band filtering can be utilized.

For noise rejection in a common-mode transducer, it would be advantageous to have a better mechanical arrangement using a coaxial arrangement of the stems of the target and dummy units, with their respective centers of mass coincident. A major improvement in rejection should also be realizable if the amplified separate signals from the target and dummy units are envelope-detected prior to subtraction.

Electrical noise and its minimization.- In a spacecraft it should be possible to make mechanical noise much lower than on earth, although there will still be such mechanical inputs as structural shifts due to thermally induced expansions and contractions, shocks due to impingement of micrometeoroids on other parts of the skin, and accelerations due to motions of parts in other experiments. If the mechanical compensation scheme described earlier is used, electrical noise may predominate in the case of the momentum transducer in the space vehicle. For a sensitivity to impact momenta on the order of 10^{-5} dyne-sec, the electrical noise generated in the transducer itself and the noise introduced by the required amplifier can be kept within tolerable limits. This can be shown in several steps as follows:

Figure 15(a) shows an extremely simplified equivalent circuit for the mechanically driven transducer followed by an amplifier with its noise sources included and then a filter. The only electrical noise source of the transducer is its leakage resistance, R_c, about 100 MΩ. The load resistance, R_L, is chosen such that maximum power transfer from a capacitive source to a resistive load will occur, which means that the absolute value of the capacitive reactance must be equal to the load resistance. This choice makes $R_L \ll R_c$ or about 2 MΩ for the prototype transducer. The load resistance R_L is shown noiseless and all amplifier noise is represented by $\overline{e_n^2}$ and $\overline{i_n^2}$, the average square voltage and current. With this simplification in mind, the circuit is further reduced by Thevenin's theorem and shown in figure 15(b). As can be seen, the noise voltage generated by R_c is reduced by $1/\sqrt{2}$ times the ratio of load to leakage resistance. For a noiseless amplifier with a gain of unity, the average voltage due to the transducer appearing at the output will be (for a bandwidth of 2.5 cps, which will be justified later, and $R_c = 50\ R_L$)

$$\sqrt{\overline{e^2}} = (4kTBR_c)^{1/2} \frac{R_L}{\sqrt{2}R_c} = 0.03 \ \mu V \tag{24}$$

while the peak signal voltage from the calibration curve (fig. 10) is 10 μV.

As an example of the noise contributed by the amplifier, the measured noise voltage and current sources for a field-effect transistor are given for the operating frequency of the transducers.

$$\sqrt{\overline{e_n^2}} = 0.069 \ \mu V/C^{1/2}$$

$$\sqrt{\overline{i_n^2}} = 0.0178 \ \mu\mu A/C^{1/2}$$

The noise voltage due to $\overline{i_n^2}$ is

$$\sqrt{\overline{e_{ni}^2}} = B^{1/2}R_L\sqrt{\overline{i_n^2}}/\sqrt{2} = (2.5)^{1/2}2\times10^6\times0.0178\times10^{-11}/\sqrt{2} = 0.0398 \ \mu V \tag{25}$$

and that due to $\sqrt{\overline{e_n^2}}$ is

$$\sqrt{\overline{e_n'^2}} = (2.5)^{1/2}0.069/\sqrt{2} = 0.077 \ \mu V$$

If one assumes that the amplifier noise sources are correlated, the total noise will be

$$\sqrt{\overline{e_{nt}^2}} = \left[\left(\sqrt{\overline{e_{ni}^2}} + \sqrt{\overline{e_n'^2}}\right)^2 + e_c'^2\right] = 0.121 \ \mu V \tag{26}$$

This is indeed small with respect to a 10 μV peak signal.

The choice of the filter bandwidth will now be justified. An impact of short duration, on the transducer target is essentially an impulse function. The spectrum of an impulse function is a constant (i.e., all frequencies are represented with the same amplitude). Thus, the relative output power spectral density for the impulse input is the same as the frequency response curve characteristic of the transducer, and the signal bandwidth to the half-power points is

$$B_t = \frac{C_d}{M} \text{ (radians/sec)} \tag{27}$$

By a rule of thumb, the filter should have about the same bandwidth as the signal. A second transducer following the amplifier and tuned to the same resonance frequency as the momentum transducer makes an excellent filter. This method of filtering was used when the calibration curve in figure 10 was obtained.

In order to achieve the above tolerable electrical noise levels, attention to details is important. Low-noise differential amplifiers having good common-mode electrical rejection are used. Wherever appropriate, batteries in place of dc power supplies are employed and a transistorized battery-powered preamplifier is attached directly to the instrument. (See fig. 2(b).) This makes possible the use of very fine enameled wire leads to interconnect the preamplifier and amplifier. These soft fine wires assist in reducing

mechanical noise transmission and are essential for applications requiring low threshold sensitivity. Since the mechanical noise in ground applications by far overshadows the electrical noise problem, electronic filtering and other electronic systems are employed to reduce mechanically induced noise. The selection of the type of electronic components and their effectiveness in noise reduction is directly dependent upon the application.

Electronic Systems and Data Reduction Techniques to Provide Low Level Impact Detection Thresholds

False alarm probability.- For measurements in the laboratory the main interest was in measuring with reasonable accuracy the momentum of an impact occurring at a known time. It was accepted, more qualitatively than quantitatively, that in order to obtain a useful measurement the signal must rise significantly above the noise level. In an application such as a micrometeoroid detector on an earth satellite or a space probe, on the other hand, one is interested in measuring the magnitude of impact momentum with fair accuracy, but one is also interested in detecting and counting impacts down to the lowest threshold level at which an impact can barely be discerned with some degree of certainty. This leads to the statistical question as to whether the noise fluctuations will be large enough to cause an objectionable number of false alarms, that is, signals that will be mistaken for 10^{-5} dyne-sec level impacts.

Noise in the momentum transducer system, shown in the block diagram in figure 16(a), comes from numerous sources, some mechanical and some electrical, as discussed previously. Because of the filtering action of both the transducer itself and of the filter following the amplifier, the output noise will almost certainly be a narrowband gaussian random process with zero mean (see refs. 8 through 11).

In this case the probability density function is

$$p[x(t)] = \frac{1}{\sqrt{2\pi}\sigma} e^{-x^2/2\sigma^2} \tag{28}$$

and

$$x(t) = V(t)\cos(\omega_o t + \theta) \tag{29}$$

where $V(t)$ is the envelope (see fig. 16(b)), ω_o the frequency of the process which is equal to the resonance frequency of the sensor, and σ^2 the mean square noise voltage of $x(t)$. The envelope follows a Rayleigh distribution

$$p(V) = \frac{V}{\sigma^2} \exp\left(-\frac{1}{2}\frac{V^2}{\sigma^2}\right) \tag{30}$$

If a threshold is selected such that any excursion of the envelope voltage above this threshold is assumed to be the result of a micrometeoroid impact, then any excursion above this threshold due to noise alone would represent a spurious count, or false alarm. For the above Rayleigh distributed

envelope the noise exceeds a threshold level V_o an average of $1/2\ \overline{N(V_o)}$ times per second, where

$$\frac{1}{2}\overline{N(V_o)} = \frac{1}{2}(8\pi\sigma^2 B_o)^{1/2}\frac{V_o}{\sigma^2}\exp\left(-\frac{1}{2}\frac{V_o^2}{\sigma^2}\right) \tag{31}$$

and B_o is the rms bandwidth of the process evaluated around its center frequency f_o,

$$B_o^2 = \frac{2\int_o^\infty (f-f_o)^2 S_x(f)df}{\int_{-\infty}^\infty S_x(f)df} = \frac{2\int_o^\infty (f-f_o)^2 S_x(f)df}{\sigma^2} \tag{32}$$

The probability density $p(V)$ has a mean of

$$m_V = \left(\frac{\pi}{2}\right)^{1/2}\sigma \tag{33}$$

and a variance of

$$\sigma_V^2 = \left(2 - \frac{\pi}{2}\right)\sigma^2 \tag{34}$$

Threshold level V_o is the independent variable of (31) and σ^2 can easily be measured. The noise σ^2 will be a slowly varying function of the spacecraft environmental factors such as temperature and parameter changes of the instrument itself. When actual inputs are very infrequent, the noise voltage can be measured continuously while the instrument is in operation and the error in the noise voltage measurement from the addition of actual inputs will be negligible. This suggests the use of a measurement of the noise voltage for control purposes. Drawn against the variable V_o, equation (31) has the shape of a Rayleigh distribution. (See fig. 16(c).) The magnitudes of V_o that are of interest are several σ's along the V_o axis. (That $N(V_o)$ is a small number for small V_o's is not of interest, since this simply means that for such a case, the noise level is almost always above V_o.)

As an example of the use of the information, let us assume that the expected number of impacts per day of a certain minimum momentum was 10. The value of V_o corresponding to such impacts on a noiseless instrument is known from the instrument sensitivity. If our calculation of the average number of crossings of the level V_o due to noise alone gives a much smaller value than 10 per day, the data can be accepted with some confidence. If, however, the noise statistics alone account for several outputs greater than V_o per day, the impact data would be questionable and the threshold should be reset to a higher value. This brings out the fact that the choice of the detection threshold of the transducer is not only a function of the noise power and the signal level, but also a function of the average rate of input signals.

With the knowledge of the noise statistics, one can now analyze the performance of the instrument and determine the optimum filter.

The narrower the passband of the filter in figure 16(a), the less noise power will be passed, but also the signal strength will be reduced. To choose a filter structure, which can be analyzed with relative ease, a single tuned amplifier stage is chosen. (See fig. 17(a).) This filter is assumed to be tuned to the resonance frequency of the transducer. Its bandwidth depends on the value of resistance. Its peak output for an exponentially decaying sinusoid is given by

$$V(t) = IR \frac{Q}{1 - Q} \left(Q^{\frac{Q}{1-Q}} - Q^{\frac{1}{1-Q}} \right) \tag{35}$$

where the ratio of filter bandwidth to transducer bandwidth is

$$Q = \frac{B_f}{B_t} \tag{36}$$

The envelopes for different bandwidths are shown in figure 17(b) and the peak amplitudes of the envelopes are plotted as a function of the bandwidth ratio Q in figure 17(c). The function has been normalized to make the steady-state output voltage $I \cdot R$ of the amplifier independent of R, and it is set equal to unity.

In the most ideal system the equivalent Johnson input noise of the amplifier would be the only noise source and

$$\sigma_{ideal}^2 = 4kTBR \tag{37}$$

To account for the actual situation we multiply by a noise figure, NF, which is a function of the amplifier as well as the environment.

$$\sigma^2 = 4kTBR(NF) \tag{38}$$

It is now possible to evaluate the effects of the filtering bandwidth and the noise factor on the false alarm rate. The output voltage of the unfiltered transducer is 10 μV for an input of 10^{-5} dyne-sec and less for filtered output according to equation (35). The values of (35) and (38) have been entered in (31) and false alarm rate curves versus bandwidth have been calculated for various noise factors for the prototype transducer.

This family of curves is shown in figure 18. Two pieces of information can be immediately read from the graph, the optimum filter bandwidth, which is about two cps, (approximately equal to B_t) and the maximum noise factor that can be tolerated without getting an excessive number of threshold crossings due to noise.

A micrometeoroid momentum detector system for low data rates.- Assume a micrometeoroid detection system utilizing a dummy transducer for mechanical noise rejection in a spin stabilized spacecraft designed for use in interplanetary space. Further the spacecraft spin axis is oriented 90° to the orbital plane and the detector principal axis is located normal to the spin axis. The instantaneous direction of the sensor is defined by the angle formed by the sensor principal axis and the sun-to-spacecraft axis. Sun sensors provide the angular reference. The presence of the dummy sensor allows a degree of noise

suppression even though the statistics of the noise are not known. The mechanical noises are introduced into the sensors through their common support structure; therefore, they are very nearly equal. The responses of the sensors, however, will differ to some degree because of the unavoidable differences in physical structure and electrical and mechanical parameters. Also the equivalent electrical noises of the amplifiers are completely uncorrelated.

In order to analyze the data taken in space so as to achieve the lowest possible detection threshold, the outputs of both sensors would have to be transmitted to earth simultaneously in analog form. With a 3-cycle bandwidth of each sensor, this would take up completely the probable 10 bits per second data rate of an interplanetary probe. Operation in such a manner would mean that the instrument can be operating only intermittently, since it must share the transmitter with other experiments on the spacecraft. As an additional burden, the gains of the two sensors would have to be checked periodically by ground command to apply pulses of equal magnitude to both sensors to measure the outputs. These problems are avoided by the system shown in figure 19. This system equalizes the relative sensitivities of the active and dummy channels and adjusts the detection threshold as a function of the noise power which is determined by an average noise power detector.

The noise outputs at points C and D will each consist of two parts, $V_C = V_1 + V_K$ and $V_D = V_2 + V_K$, where V_K is the common-mode signal due to mechanical disturbances, V_1 and V_2, the electrical noises, will be independent and will, in general, have slightly different noise powers, that is,

$$\sigma_{V_1}^2 \neq \sigma_{V_2}^2$$

By measuring E the difference of the outputs at C and D and adjusting the gain of one of the sensor amplifiers so that the average of $V_C - V_D$ is zero, σ_{V_1} and σ_{V_2} are made equal. The average uncompensated noise power at E (e.g., ref. 11) is then:

$$\overline{(V_C - V_D)^2} = \overline{[V_1 + V_K - (V_2 + V_K)]^2} = \overline{(V_1 - V_2)^2} = \sigma_{V_1}^2 + \sigma_{V_2}^2 = 2\sigma_{V_1}^2 \qquad (39)$$

For the system in figure 19, therefore (using eq. (34))

$$E(V) = 0 \qquad (40)$$

$$\sigma_V^2 = 2\left(2 - \frac{\pi}{2}\right)\sigma^2 = (4 - \pi)\sigma^2 \qquad (41)$$

Where V is defined as

$$V \equiv V_1 - V_2 \qquad (42)$$

The new probability density for the amplitude of $V_1 - V_2$ can be found by convolution of the probability densities (see fig. 20(a))

$$p(V) = \int_{-\infty}^{\infty} p_{V_1}(v)\, p_{V_2}(v - V)\, dv \qquad (43)$$

giving the following result

$$p(V) = \frac{1}{2\sigma}\left(1 - \frac{V^2}{2\sigma^2}\right) e^{-V^2/4\sigma^2} \text{Erfc}\left(\frac{V}{2\sigma}\right) + \frac{V}{4\sigma^2} e^{-V^2/2\sigma^2} \tag{44}$$

where the coerror function is defined as

$$\text{Erfc} \equiv \int_{V/2\sigma}^{\infty} e^{-v^2}\, dv \tag{45}$$

and $p(V)$ is almost gaussian. (See fig. 20(b).) If one assumes the gaussian approximation to be valid, the average number of times the threshold is exceeded can also be found from

$$\frac{1}{2}\overline{N_V(V_o)} = \frac{1}{2}\int_{-\infty}^{\infty} |\dot{V}|\, p(V_o, \dot{V})\, dv \tag{46}$$

where $\dot{V}$ is the derivative of the random variable V_o with the result

$$\frac{1}{2}\overline{N_V(V_o)} = B_V e^{-V_o^2/2\sigma_V^2} \tag{47}$$

B_V is the rms bandwidth of the detected and summed noise voltages (eq. (32) noting that $f_o = 0$) and is approximately equal to the rms bandwidth of the sensor itself. The exact value can be found by measuring the average rate of axis crossings since

$$\overline{N_V(o)} = 2B_V \tag{48}$$

The threshold adjustment of target and dummy transducer can then be set to give an error rate that is a certain small fraction of the expected impact rate, and, in principle, the problem is solved.

Figure 21 shows signals in the detector for various situations. It will be noted in figure 21(e) that a negative as well as a positive threshold is provided. If the instrument works properly, negative threshold crossings should be equal to the expected error rate. Therefore, this type of information is also telemetered and serves as a trouble indicator.

The operation of the instrument will now be described for four possible situations:

I. Occurrence of an actual impact

II. No impact occurring, output due to small mechanical noise and electrical noise only

III. No impact occurring, output due to a large mechanical noise or electrical pulse common to target and dummy (false alarm)

IV. No impact occurring, output due to the fact that target minus dummy noise exceeds the negative threshold (excessive noise indication)

Situation I: For this description it is assumed that the spacecraft has come to a thermal equilibrium and the average noise power detector has adjusted the instrument in such a manner that the small thermal and residual mechanical noises of random nature will not exceed the threshold and, therefore, will not cause a false output (false alarm). The signals existing at points A, B, C, and D of figure 19 are shown in figure 21, column I.

Upon an actual impact on the target, the output of the target sensor increases while the output of the dummy sensor remains undisturbed. (For the amplified and filtered outputs, see column I of figs. 21(a) and (b), hereafter referred to as 21(a)I, 21(b)I, etc.) In addition to removing most of the amplifier noise, the narrow band filters cause the gradual rise of the waveforms, as compared to the sharp rise of the sensor output waveform. The outputs of the sensor and dummy after detection are shown in figures 21(c)I and (d)I. When the difference between the output of the target sensor and the dummy sensor exceeds the controlled threshold of the instrument (fig. 21(e)I), a start pulse is generated which starts an analog-to-digital converter of the "up and down counting" type (number 1, fig. 19), which digitizes the compensated signal and automatically stops when the signal begins to decrease. At this time the first analog-to-digital converter puts out a "hold" pulse to the remaining three storage units which now store information on the magnitude of the target output voltage, the threshold setting of the instrument, and the direction of the impact. The complete information forms a 12-digit word. This word is stored temporarily and is shifted out sequentially to the telemetry system when the telemetry applies a "read-out" pulse to the sequencer unit. As shown in figures 21(c)I and 21(e)I, the ratio of the target-minus-dummy output and the uncompensated target output will be approximately unity, indicating a high probability that this truly was an impact on the target.

Situation II: When small random mechanical and electrical noises are present, only the mechanical noise components of figures 21(c)II and (d)II tend to subtract while the electrical components of the noise from the target and dummy are completely uncorrelated. The difference output at point E figure 19 will be close to zero. Analog-to-digital converter number 2 is also of the "up-and-down counting" type and follows the waveform of the uncompensated signal continuously. Upon receiving the telemetry read-out pulse, and if the storage units are not already holding data from a threshold crossing, the A-to-D converter number 1 immediately sends a "hold" signal to all of the storage units. The first four digits from A-to-D converter number 1 will be 1000, indicating that there was no impact at this time. The next three digits will indicate the noise level of the instruments as derived from analog-to-digital-converter number 2. The last five digits will represent the instrument threshold setting and look angle at the time of the read-out pulse from the telemetry. Thus even though actual data had not been taken, a history of the threshold and the noise is transmitted to earth to aid in the evaluation of the data.

Situation III: A third type of output may be generated when the threshold is exceeded by a very high mechanical noise or by electrical pulse inputs from the spacecraft (as for example, from relay closures, flipping of magnetometers, or impacts of micrometeoroids on other parts of the spacecraft). For large simultaneous mechanical disturbances of both the dummy and target the difference between the two outputs may still be positive and large enough to

exceed the threshold setting of the instrument, thus causing A-to-D converter number 1 to accumulate a reading. For the case shown in figure 21, column III, however, A-to-D converter number 2 would indicate a large output. The large difference between the uncompensated output and the difference output indicates that the reading does not result from an actual micrometeoroid impact of small magnitude, but rather from a disturbance common to both target and dummy. This example shows the usefulness of the output of the second A-to-D converter for preventing false-alarm errors.

Situation IV: In the fourth situation the dummy output exceeds the target output sufficiently that the difference in the signal will cross the negative threshold of the instrument. (See fig. 21, column IV.) If the instrument works properly, such occurrences should be extremely rare. This type of output is mainly an indication of excessive noise. When an approximately equal amount of positive and negative outputs are recorded, either the threshold setting was too low, or both dummy and target piezoelectric beams are developing spurious outputs. The output to the telemeter will be of exactly the same form as described in Situation I except for the fact that the presence of a "0" in the first bit from A-to-D converter number 1 will indicate a negative output.

It can be seen that most of the data reduction has been performed in the instrument package. For a low expected impact rate of one impact per day, a readout of the 12-digit word every 5 minutes will be sufficient to give, in addition to the actual impact data, a history of the threshold settings and noise statistics of the instrument.

ADDITIONAL APPLICATIONS

In addition to the initial purpose of detecting and measuring micrometeoroid impacts, the unique characteristics of this transducer make it applicable to a wide variety of uses.

The use of the transducer for measuring the energy in the light pulses from a laser has been reported in reference 12. The transducer not only provides a means for measuring laser energy but also provides a research tool for investigating laser impact phenomena.

Although the instrument by its inherent design (piezoelectric effect) is primarily of the dynamic type, it can be used for measuring a steady force-producing medium (i.e., light, electron, or ion beam). This is accomplished by interrupting or chopping the medium at the natural frequency of the instrument. Since the instrument is driven at its natural frequency, its sensitivity is increased relative to the static deflection. The relative magnification relationship is shown in table II. At the Ames Research Center the Physics Branch has used the transducer for measuring the forces on ion-bombarded surfaces. A transducer with integral calibrator is used for this research. Since the transducer is directionally sensitive, it is possible to orient a target parallel to the principal axis of the transducer and thereby measure a tangential component of force.

One novel application of the transducer in biomedical research is in the measurement of the heartbeat of an avian embryo. The transducer as shown in figure 2 is converted to a ballistocardiograph simply by attaching a cup to the transducer stem to support the egg. Details for this application are given in reference 13. The ballistocardiograph is believed to have a wide application in the study of the effects of drugs, chemicals, pesticides, and environmental factors on a variety of small animal life. The heartbeat rate has been observed in young chickens, rats, cockroaches, and snails.

The transducer can be employed as a narrow band electromechanical filter without any alterations whatsoever. This is accomplished simply by applying the signal to be filtered to one of the piezoelectric beams and taking the filtered signal from the other beam. Typical response characteristics are shown in figure 22.

Another capability which became quite obvious (and the source of a problem) early in the development of the instrument was its seismometer characteristics. This feature was utilized in determining environmental noise conditions for evaluating suitable test locations for the transducer.

CONCLUSIONS

Tests of the piezoelectric momentum transducer as an impulse detector using low-velocity, short-duration, and hypersonic impacts indicate the following conclusions.

1. The transducer output is directly proportional to the component of impact momentum transferred to the target in a direction parallel to the transducer principal axis.

2. The sensitivity of the transducer is essentially independent of the location of impact on the target area.

3. The transducer and associated electronics can be calibrated at various momentum levels by a remote process which lends itself to applications for space vehicles.

In addition, the unique characteristics of the transducer permit wide variety of uses. It has been used with excellent success at the Ames Research Center for

1. A narrow band-pass electrical mechanical filter

2. An ultrasensitive vibration pickup

3. A laser energy calibrator and impact transducer

4. A force transducer for measurement of ion-beam accommodation factor

5. A ballistocardiograph for measurement of motion of small living organisms or components such as heartbeat reactions.

Ames Research Center
National Aeronautics and Space Administration
Moffett Field, Calif., April 5, 1965

APPENDIX A

BEAM ELECTRODE SEPARATION

It was pointed out in the section on transducer voltage response that the sensor beam deformation produced a moment distribution which would cancel the voltage if the electrodes were not separated at the midspan. Reviewing the moment distribution, or stress, and considering the fact that charge developed is directly proportional to stress, one may note that the maximum charge developed occurs at the fixed ends of the beam and is zero at the midspan. Thus it appears that a higher open-circuit voltage could be obtained if only the more highly stressed portions of the beam were used. However, any reduction in the electrode area causes a reduction of the beam capacitance and hence increases the impedance of the transducer. It was therefore of interest to determine the output of the transducer for various values of load impedance as a function of the amount of electrode area removed. The computed results obtained by use of the simplified equivalent circuit are shown in figure 23. It appears from these results that for realistic loads the amount of electrode area removal is not critical.

APPENDIX B

ELECTRICAL EQUIVALENT CIRCUIT

For any detailed analysis of the dynamic behavior of the transducer and its associated electrical circuits it is desirable to obtain an electrical equivalent circuit of the transducer. The electromechanical equivalent circuit for a simple piezoelectric cantilever beam suspension with concentrated mass at the end was shown in table I. As was also stated in the section on transducer design considerations, the electrodes of the beam sensors are separated at the midspan. Thus, in essence, there are four electrically independent elements, and the electromechanical equivalent circuit of the transducer should be drawn as in figure 24(a). As in table I, the primed quantities refer to the typical cantilever beam, whereas the unprimed quantities refer to the actual configuration of the transducer beams. The analysis of this circuit combined with any attached external circuitry describes the complete electrical and mechanical behavior of the transducer. As normally operated, two of the sensor circuits are connected in parallel, with appropriate polarities, to provide the output signal, while the terminals of the other two are short-circuited to eliminate induced electrical noise. For this particular arrangement the equivalent circuit is shown in figure 24(b), where the transformers have also been eliminated with appropriate adjustment of circuit element values by the square of the turns ratio. As viewed from the electrical terminals, the transducer behaves exactly like a low-loss parallel resonant circuit with a capacitor C_e in series. To confirm the validity of the analogy, impedance measurements of the transducer as a function of frequency were made by means of an impedance bridge. These results are shown in figure 25. The nearly constant reactance due to C_e was subtracted before plotting to show more clearly the parallel resonance effects of the mechanical circuit on the electrical impedance.

REFERENCES

1. Dubin, Maurice: Meteoritic Dust Measured From Explorer I. Planet. Space Sci., vol. 2, no. 2/3, April 1960, pp. 121-129.

2. Myklestad, Nils Otto: Vibration Analysis. McGraw-Hill Book Co., Inc., 1944, pp. 45-48.

3. Cohen, H. A.; Corman, A.; and Dubin, M.: Calibration of Micrometeorite Detectors Used in Satellites and Rockets. Proceedings of Third Symposium on Hypervelocity Impacts, vol. I, Armour Research Foundation, Chicago, 1958.

4. Rogallo, Vernon L.; and Savage, Howard F.: Two-Component Microbalance for Measuring the Forces on Ion-Bombarded Surfaces. Rev. Sci. Instr., vol. 34, no. 9, Sept. 1963, pp. 988-991.

5. Goettelman, R. C.; Softky, S. D.; Arnold, J. S.; and Farrand, W. B.: The Meteoroid and Cosmic-Ray Environments of Space Vehicles and Techniques for Measuring Parameters Affecting Them. Wadd Rep. TR 60-486, Stanford Research Institute, Feb. 1961.

6. Friichtenicht, J. F.: Two-Million-Volt Electrostatic Accelerator for Hypervelocity Research. Rev. Sci. Instr., vol. 33, no. 2, Feb. 1962, pp. 209-212.

7. Shelton, H.; Hendricks, C. D., Jr.; and Wuerker, R. F.: Electrostatic Acceleration of Microparticles to Hypervelocities. J. Appl. Phys., vol. 31, no. 7, July 1960, pp. 1243-1246.

8. Davenport, W. B., Jr.; and Root, W. L.: An Introduction to the Theory of Random Signals and Noise. McGraw-Hill Book Co., Inc., 1958, pp. 158-167.

9. Abramson, N.; and Farison, J.: On Statistical Communication Theory. TR No. 2005-1, Stanford Electronics Laboratories, 1962.

10. Middleton, David: An Introduction to Statistical Communication Theory. McGraw-Hill Book Co., Inc., 1960, pp. 426-437.

11. Fraser, Donald Alexander Stuart: Statistics: An Introduction. John Wiley and Sons, Inc., 1958, pp. 91-109.

12. Neuman, Frank: Momentum Transfer and Cratering Effects Produced by Giant Laser Pulses. Appl. Phys. Letters, vol. 4, no. 9, 1964, pp. 167-169.

13. Rogallo, Vernon L.: Measurement of the Heartbeat of Bird Embryos With a Micrometeorite Transducer. NASA SP-5007, 1964.

TABLE I.- PIEZOELECTRIC BEAM PHYSICAL DIMENSIONS, DYNAMIC PARAMETERS FOR CANTILEVER MOUNTING, AND ELECTROMECHANICAL EQUIVALENT CIRCUIT

Beam width	$w = 0.063$ in. $\pm$ 0.003 in.
Thickness	$t = 0.026$ in. $\pm$ 0.002 in.
Voltage/force	$N' = 0.56 \frac{L'}{wt}$ (V/newton)
Capacitance of beam	$C_e' = 450 \frac{L'w}{t}$ (uuF)
Mechanical compliance	$C_m' = 3.6\ 10^{-9} \frac{L'^3}{wt^3}$ (m/newton)
Effective mass of beam	$m_b' = 0.025\ L'wt$ (kg)
Mass of target and stem	M (kg)
Hole diameter	d = 0.0075
Spacing, centers	a = 0.0125

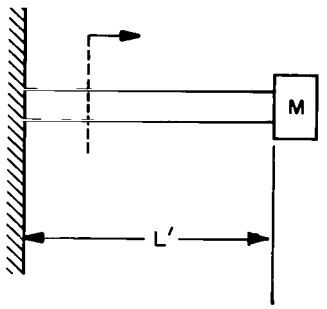

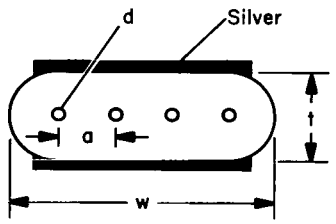

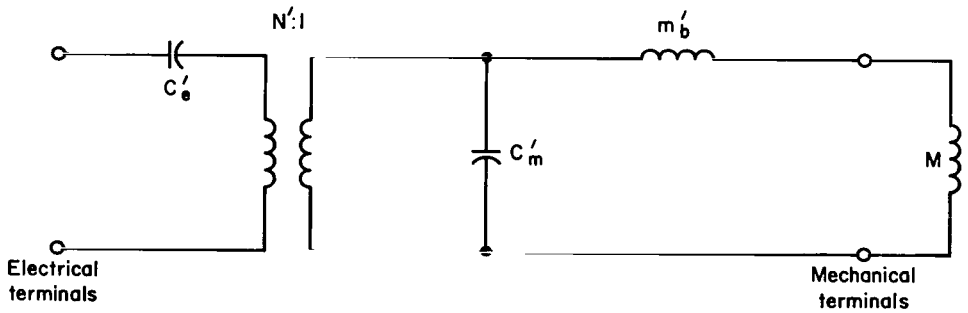

(Note: Dimensions of L', w, a, d, and t are in inches.)

TABLE II.- SOLUTIONS OF THE COMPLETE EQUATION OF MOTION FOR VARIOUS TYPES OF DRIVE FORCE

Driving function		Approximation	Initial conditions x_o	Initial conditions $\dot{x}_o$	Solution	Explanation of symbols
I Free vibration	$f(t) = F$ $t < 0$ $f(t) = 0$ $t > 0$	$C_d = 0$	$x_o = \frac{F}{K}$	0	$x = x_o \cos \omega_n t$	$\omega_n = \left(\frac{K}{M}\right)^{1/2}$
II Damped free vibration		$\left(\frac{C_d}{2M}\right)^2 < \frac{K}{M}$	$x_o = \frac{F}{K}$	0	$x = x_o e^{-\frac{C_d}{2M}t}\left(\cos \omega_o t + \frac{C_d}{2M\omega_n} \sin \omega_o t\right)$	$\omega_o = \left[\frac{K}{M} - \left(\frac{C_d}{2M}\right)^2\right]^{1/2}$
		$\left(\frac{C_d}{2M}\right)^2 \ll \frac{K}{M}$ $\frac{C_d}{2M\omega_o} \ll 1$			$x = x_o e^{-\frac{C_d}{2M}t} \cos \omega_n t$	$\omega_n = \omega_o = \left(\frac{K}{M}\right)^{1/2}$
III Forced vibration with damping		Transients have died out				$x_o = F_o[(C_d\omega)^2 + (K - M\omega^2)^2]^{-1/2}$ $\omega_{max} = \left(\frac{K}{M} - \frac{C_d^2}{2M^2}\right)^{1/2}$ $\varphi = \tan^{-1} \frac{C_d\omega}{K - M\omega^2}$
a) general	$f(t) = F_o \sin \omega t$				$x = x_o \sin(\omega t - \varphi)$	
b) simplified		$\frac{1}{2}\left(\frac{C_d}{M}\right)^2 \ll \frac{K}{M}$				$^{\dagger}\omega_{max} = \left(\frac{K}{M}\right)^{1/2}$ $x_{o_{max}} = \frac{F_o}{\omega_{max} C_d}$
IV True impulse	$f(t) = p\delta(t)$		0	$\dot{x}(0+) = \frac{P}{M}$	$x = x_1 e^{-\frac{C_d}{2M}t} \sin \omega_o t$	$x_1 = \frac{\dot{x}_o}{\omega_o} = \frac{P}{M\omega_o}$ $\omega_o = \left[\frac{K}{M} - \left(\frac{C_d}{2M}\right)^2\right]^{1/2}$
V Rectangular approximation to an impulse of momentum p	$f(t) = \frac{P}{\tau}[u(t) - u(t) - \tau]$	$\omega_o \approx \omega_n$	0	0	for $t > \tau$ $x = \frac{P}{\tau M\omega_o^2}\left[e^{-\frac{C_d}{2M}(t - \tau)} \cos \omega_o(t - \tau) - e^{-\frac{C_d}{2M}t} \cos \omega_o t\right]$	

†Relative magnification $= \frac{x_{o_{max}}}{x_{static}} = \frac{(KM)^{1/2}}{C_d}$

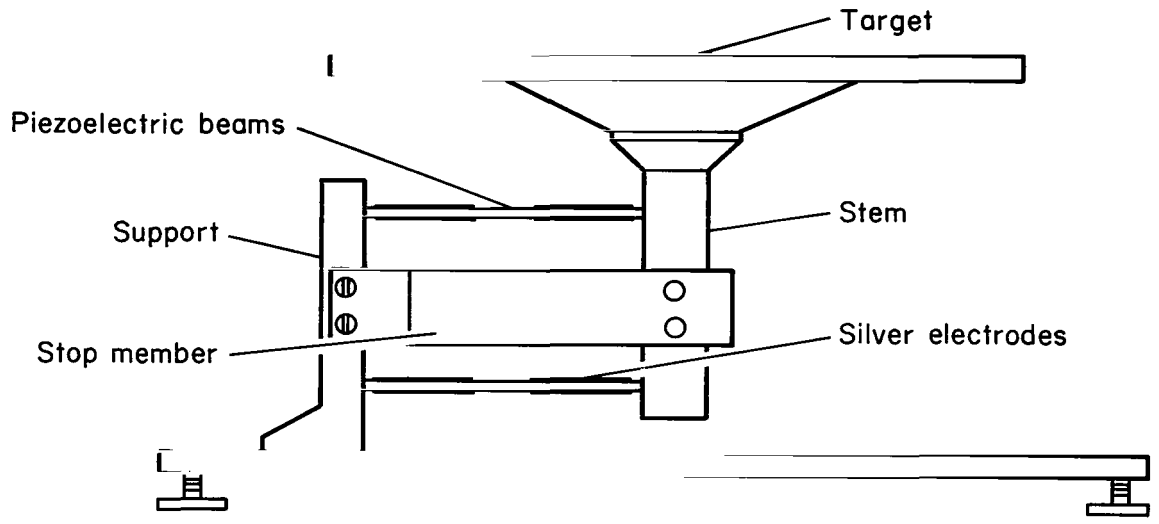

(a) Transducer general arrangement.

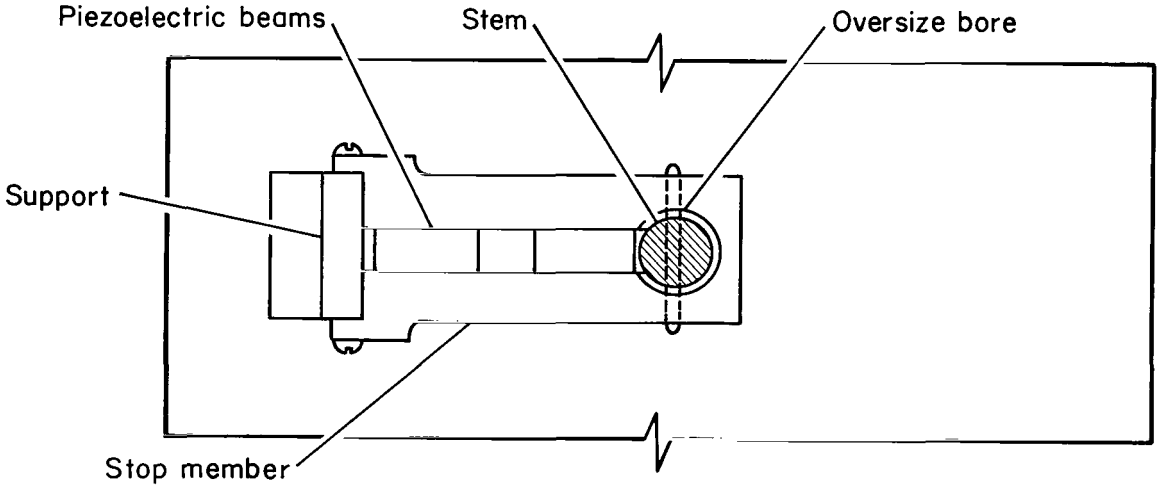

(b) Lateral and transverse torsion stop arrangement.

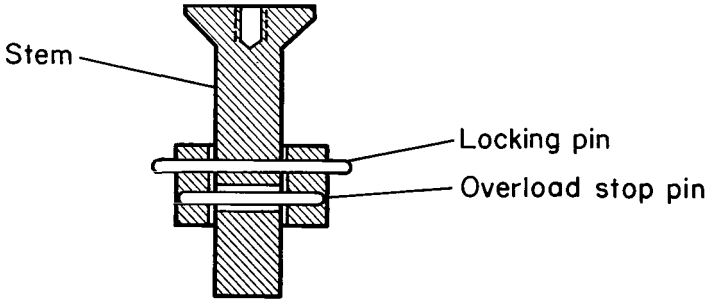

(c) Lock and overload stop limits.

Figure 1.- Components of the momentum transducer.

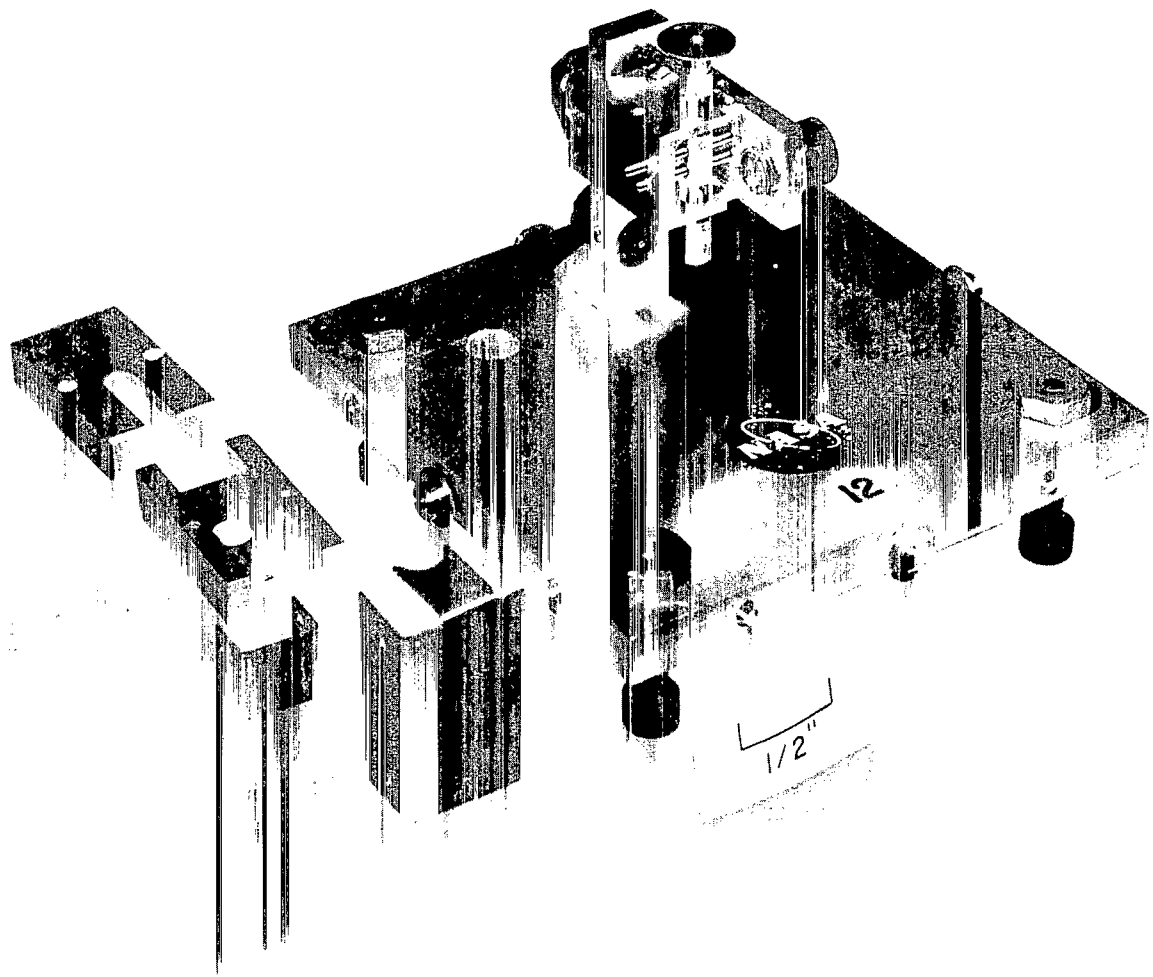

A-31977

(a) Transducer with shielding removed.

Figure 2.- Prototype momentum transducer.

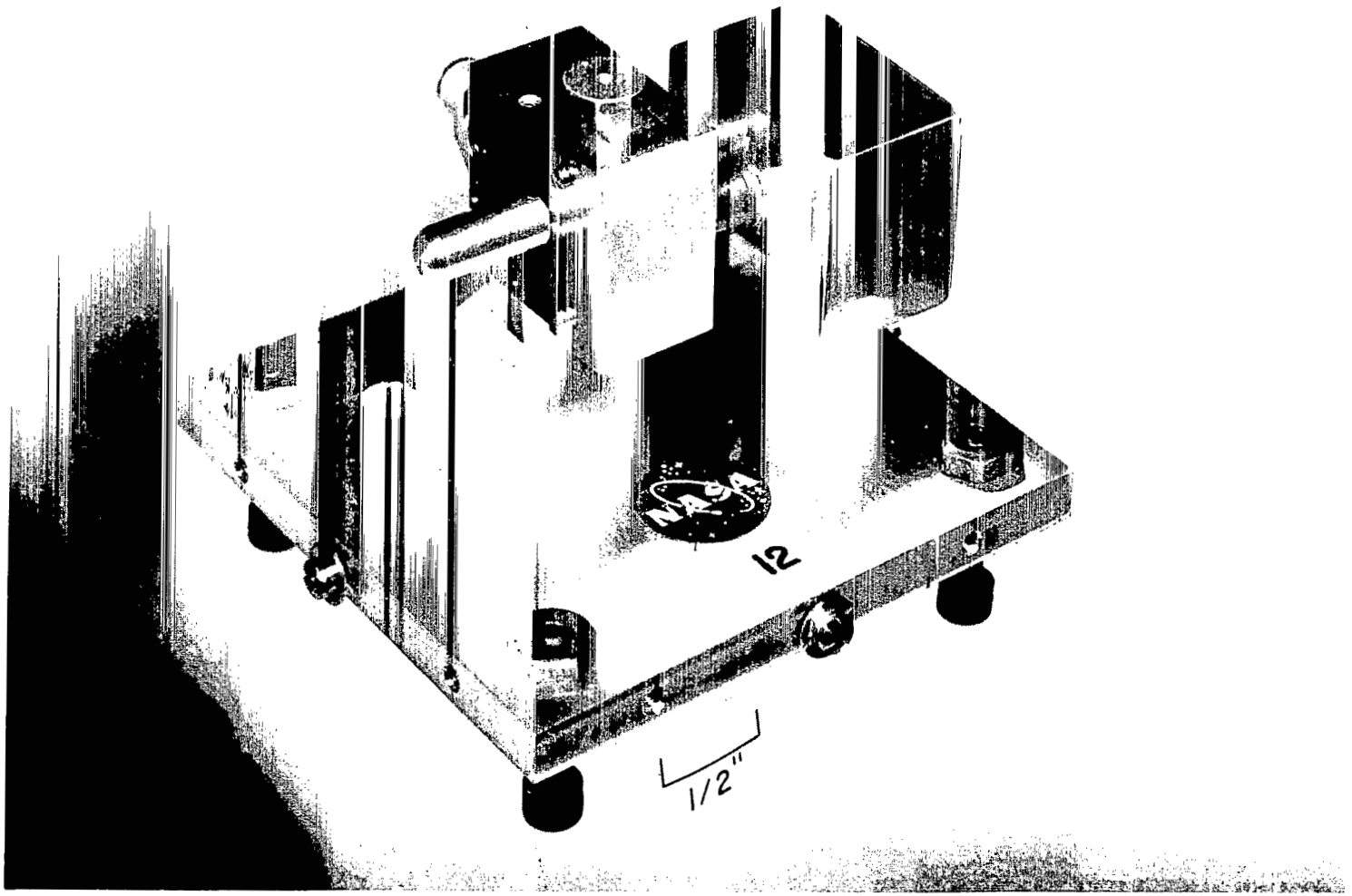

A-31975

(b) Assembled transducer with preamplifier attached.

Figure 2.- Concluded.

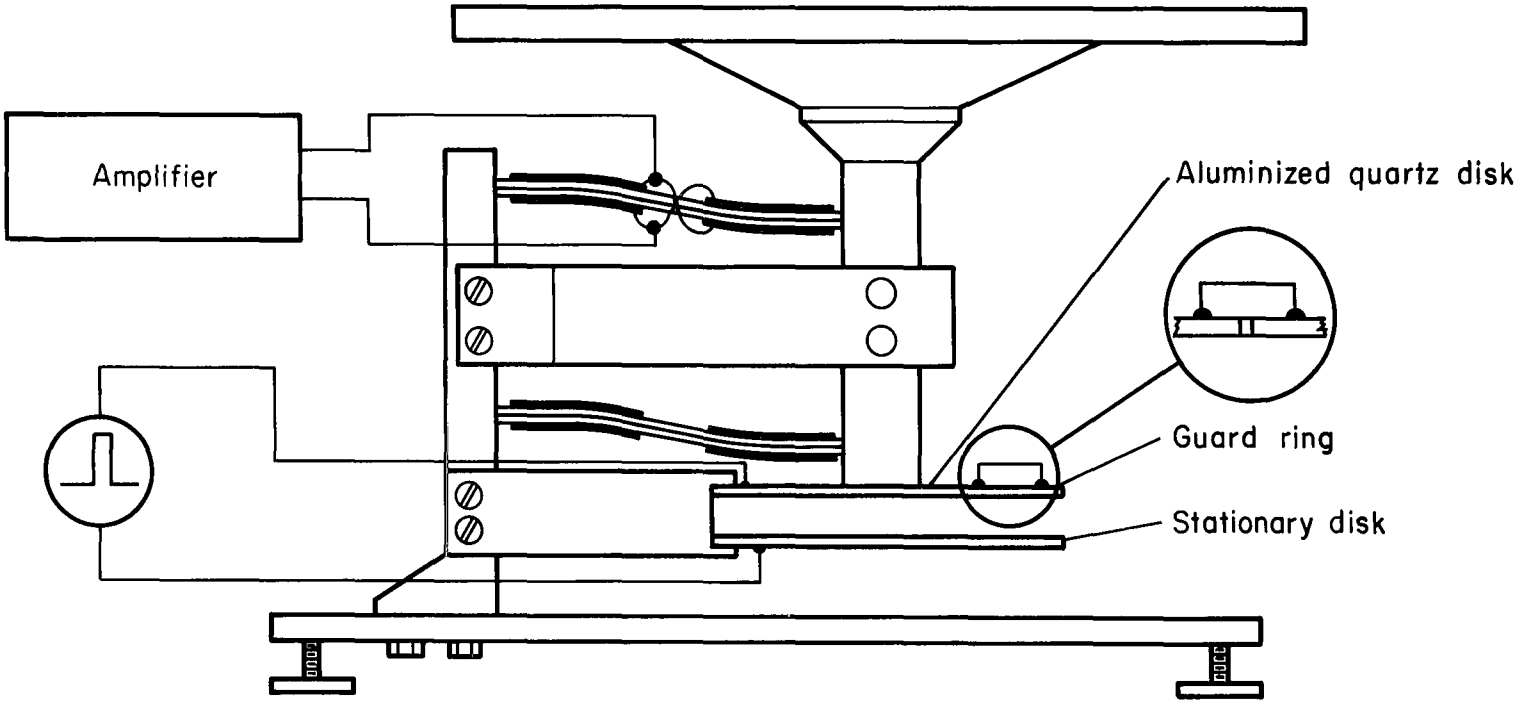

(a) Schematic arrangement of the calibrator unit.

Figure 3.- Prototype momentum transducer with integral absolute calibrator.

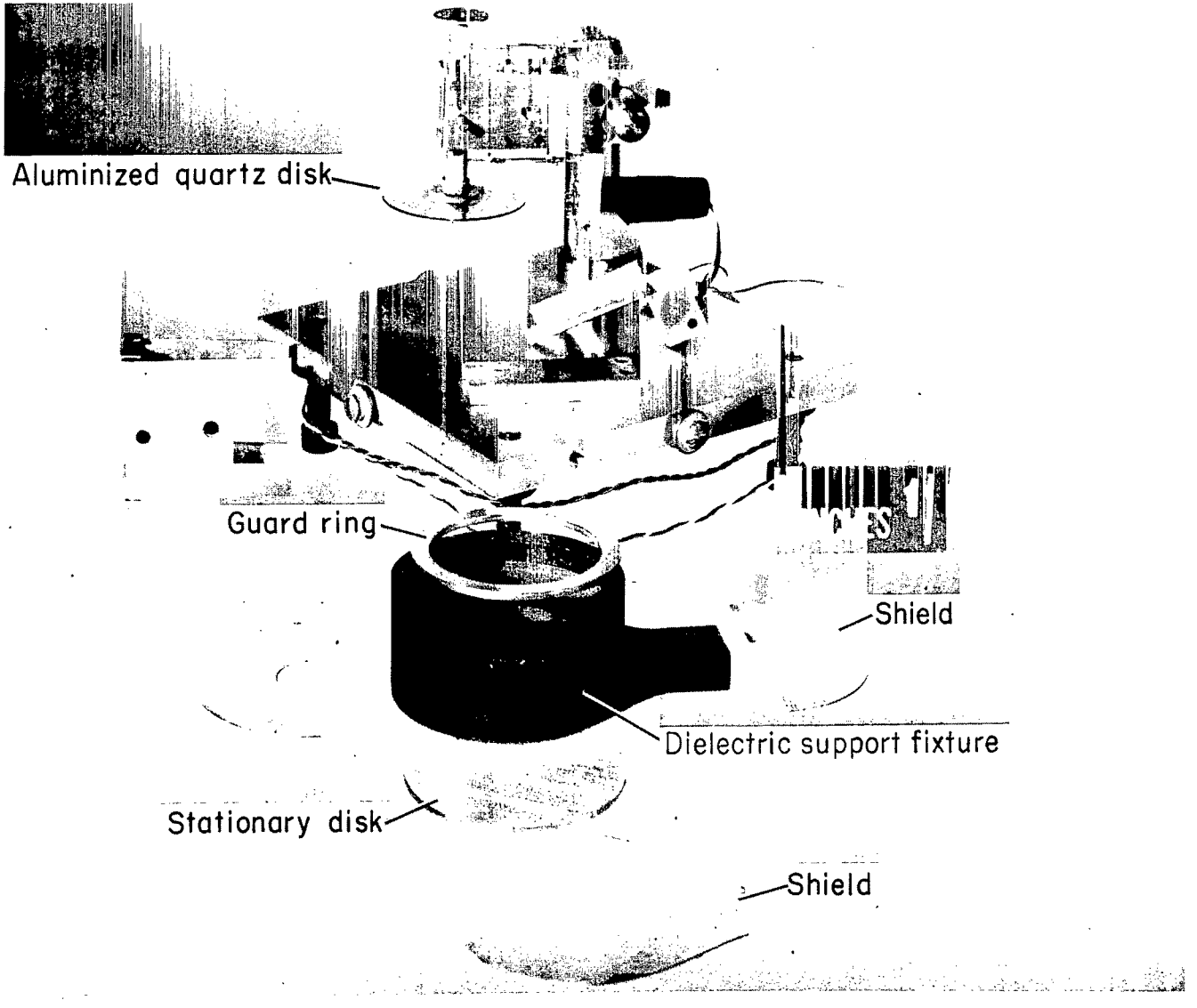

A-30766.1

(b) Transducer with aluminized quartz disk attached; shielding and fixed members of electrostatic unit removed.

Figure 3.- Continued.

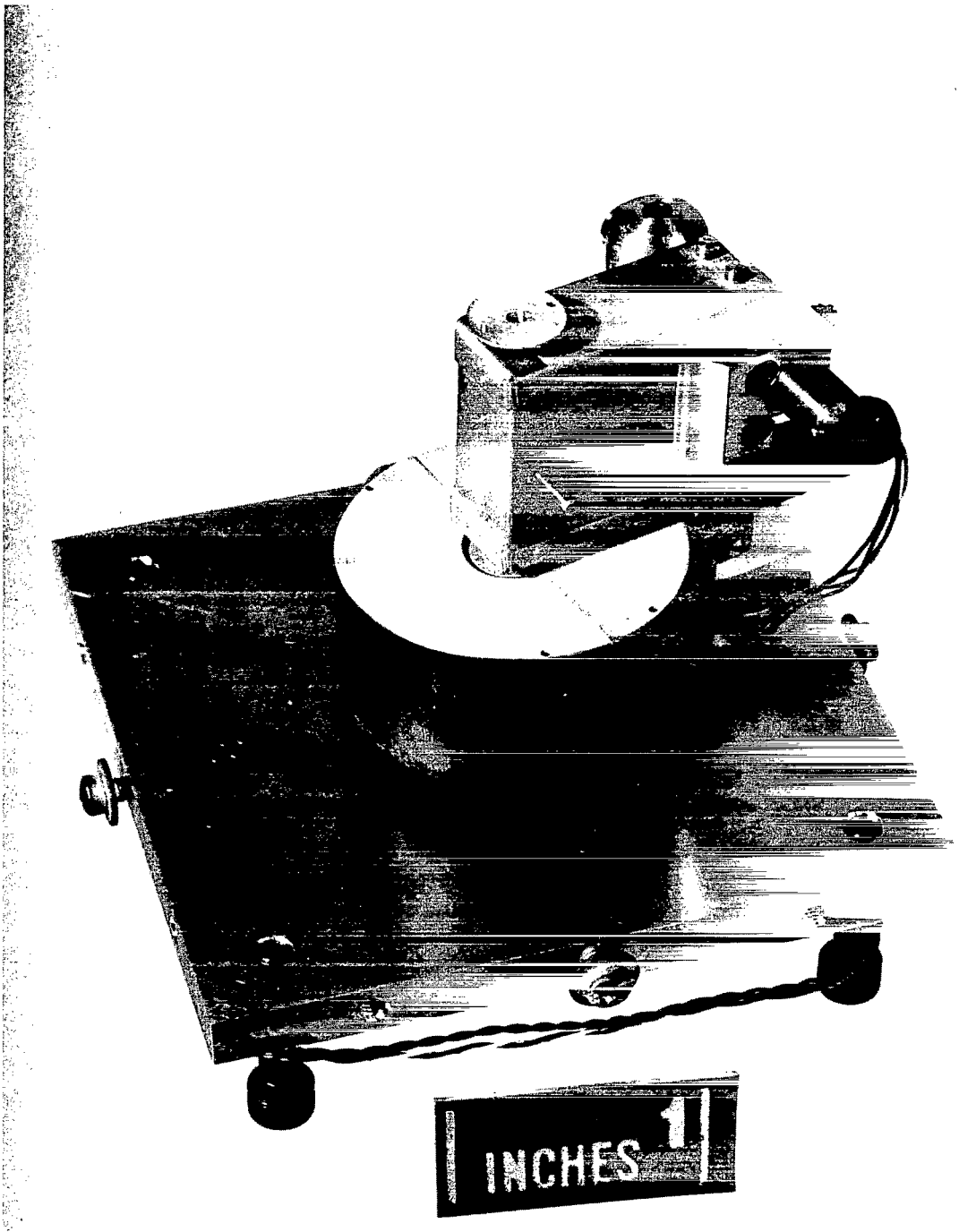

A-30768

(c) Assembled transducer with integral absolute calibrator.

Figure 3.- Concluded.

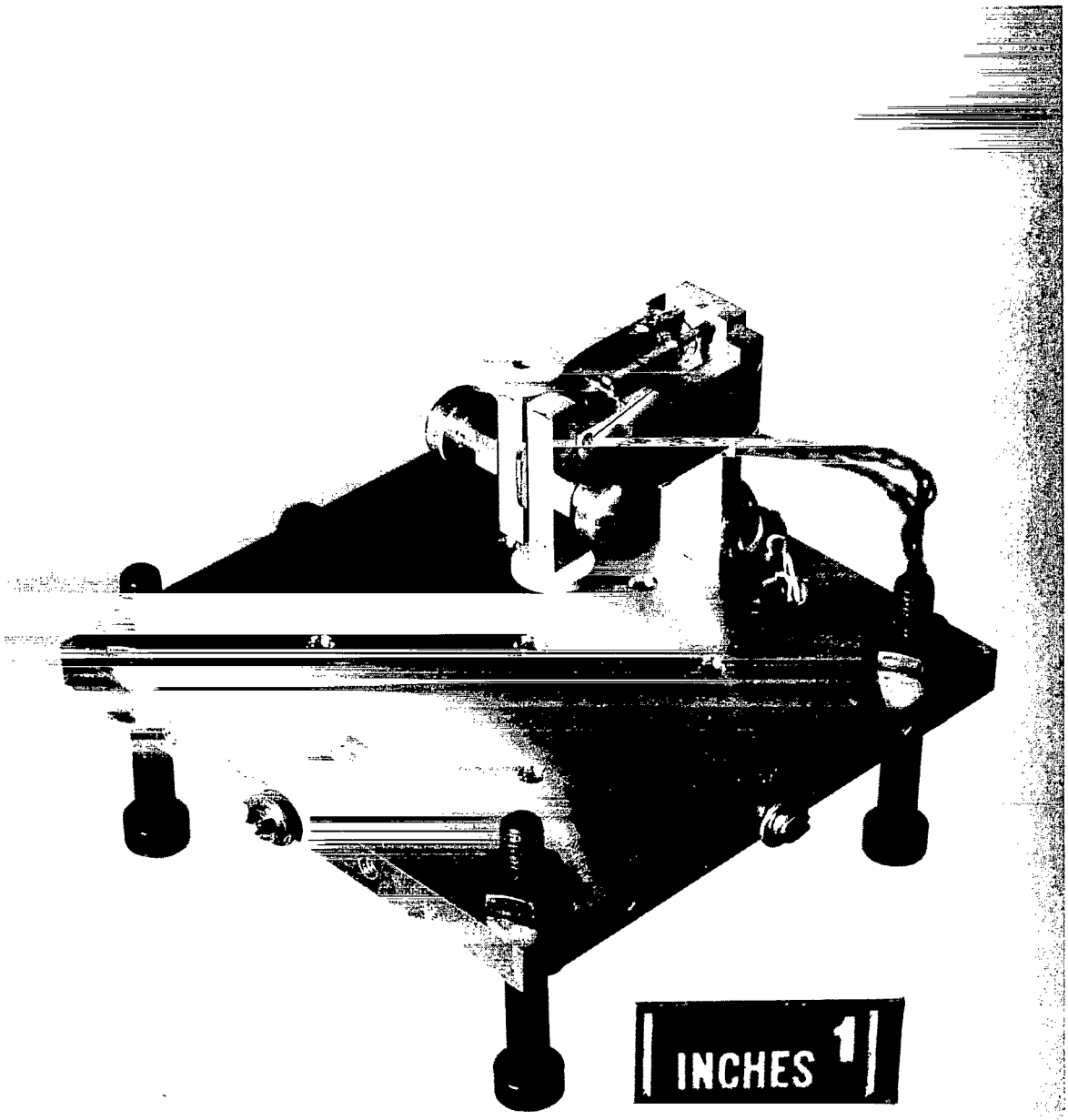

A-30764

Figure 4.- Prototype momentum transducer with mechanical noise common-mode rejection feature.

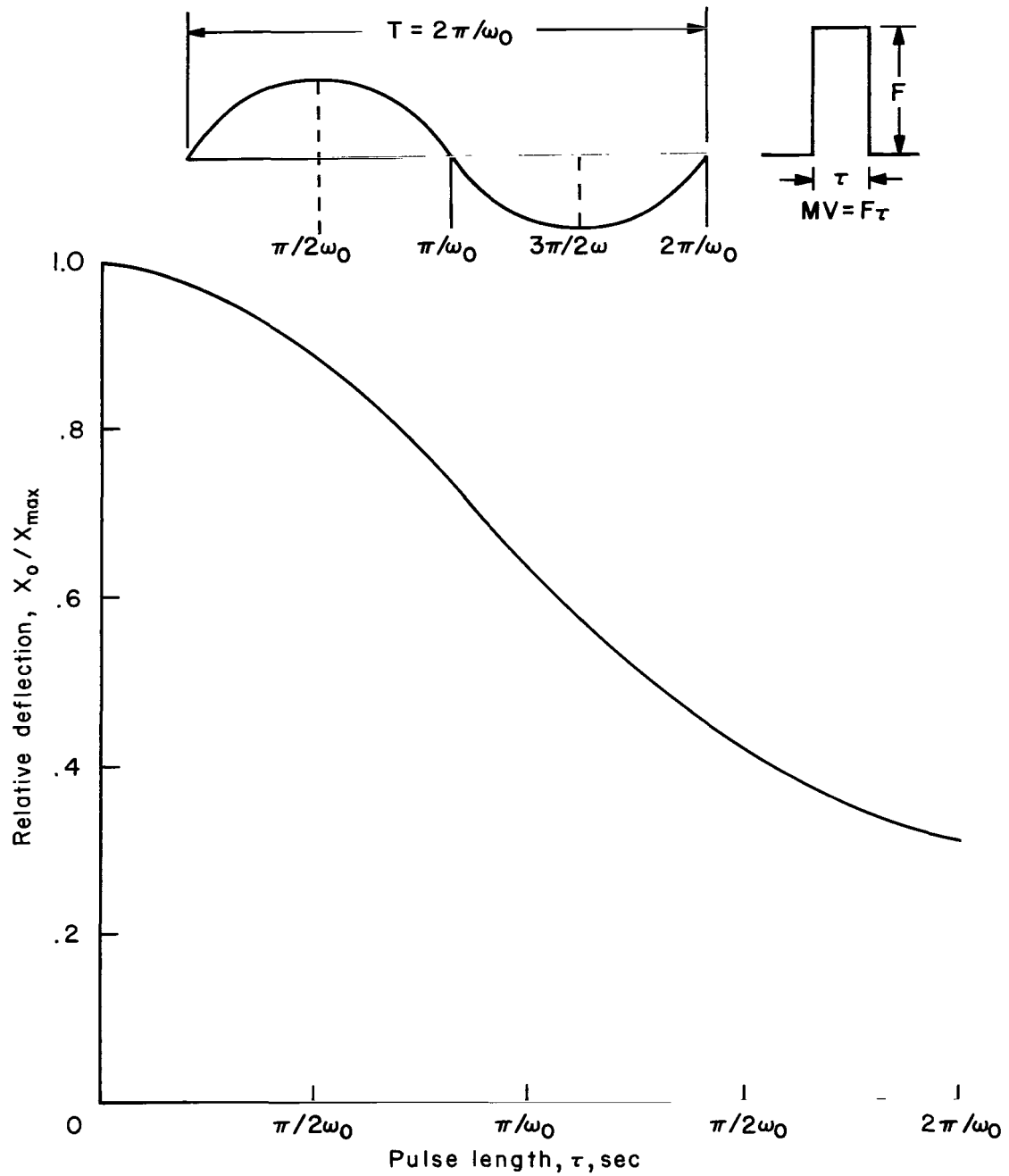

Figure 5.- Transducer response as a function of the pulse duration for a rectangular force waveform of constant momentum.

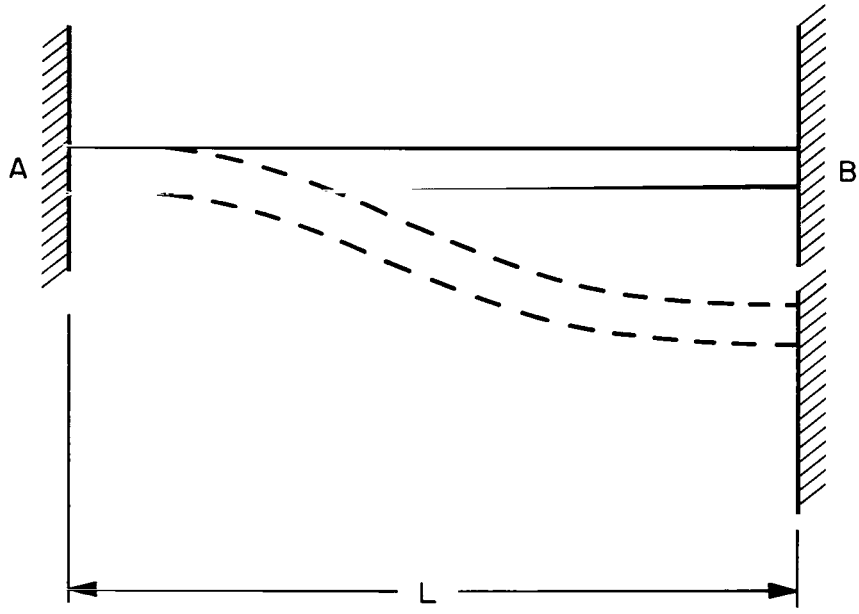

(a) Fixed-end beam with one end displaced.

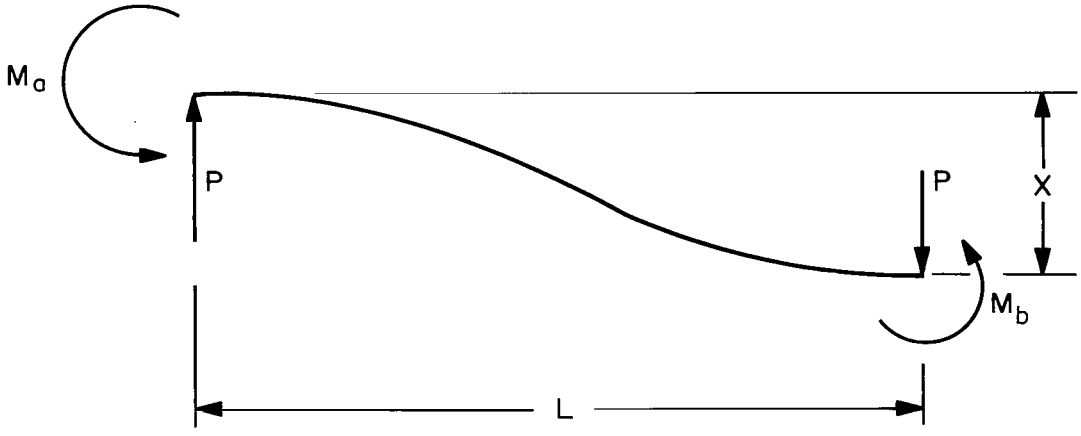

(b) Free body diagram of (a).

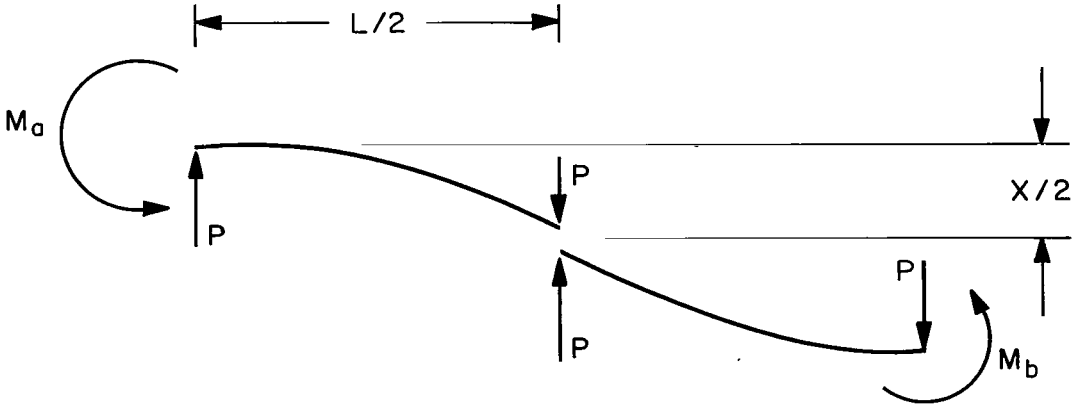

(c) Free body diagram of two cantilever beams equivalent to (b).

Figure 6.- Transducer beam distortion - deflection relationships.

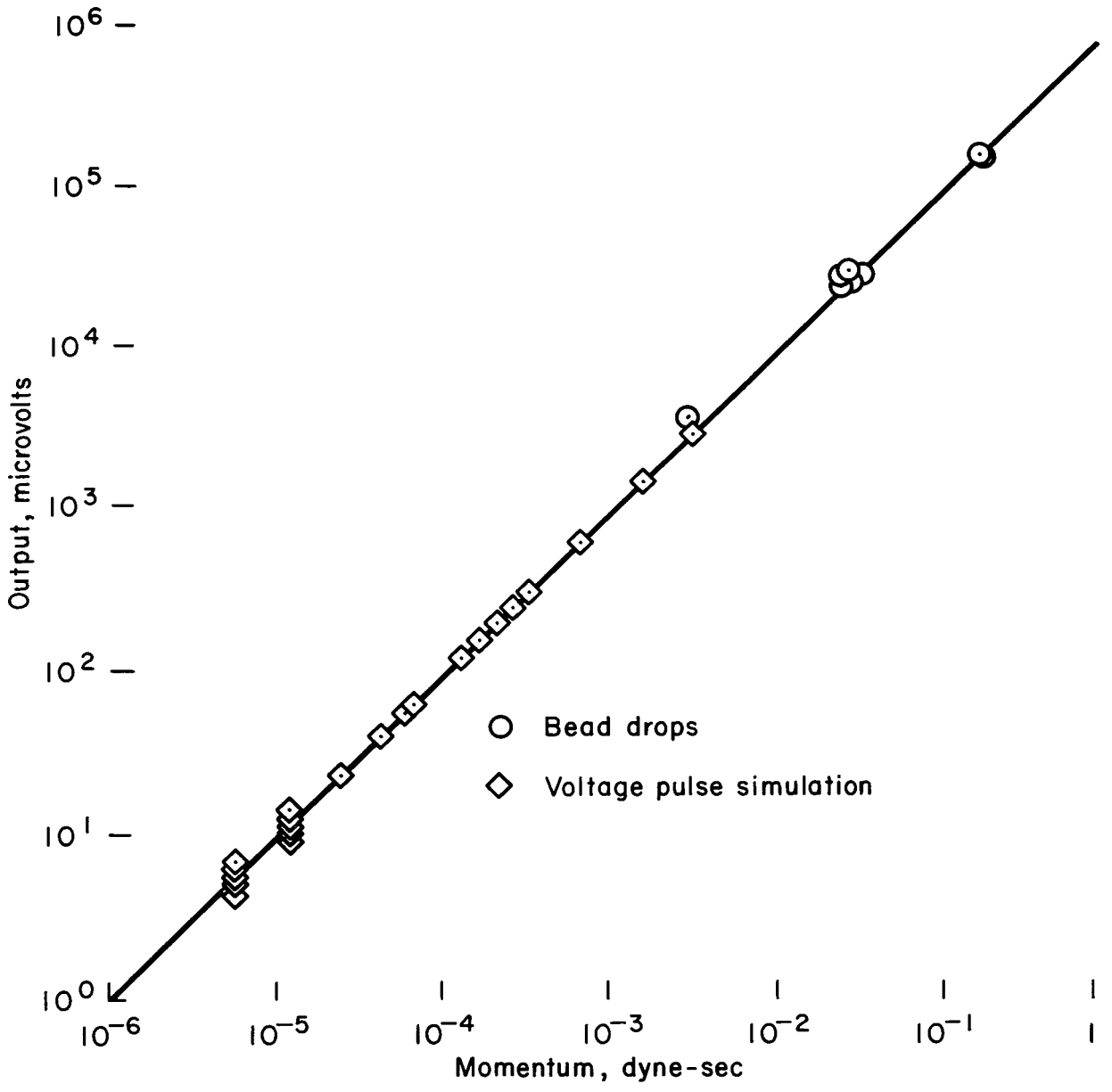

Figure 7.- Transducer momentum calibration curve obtained by the bead-drop and controlled-induced-displacement techniques.

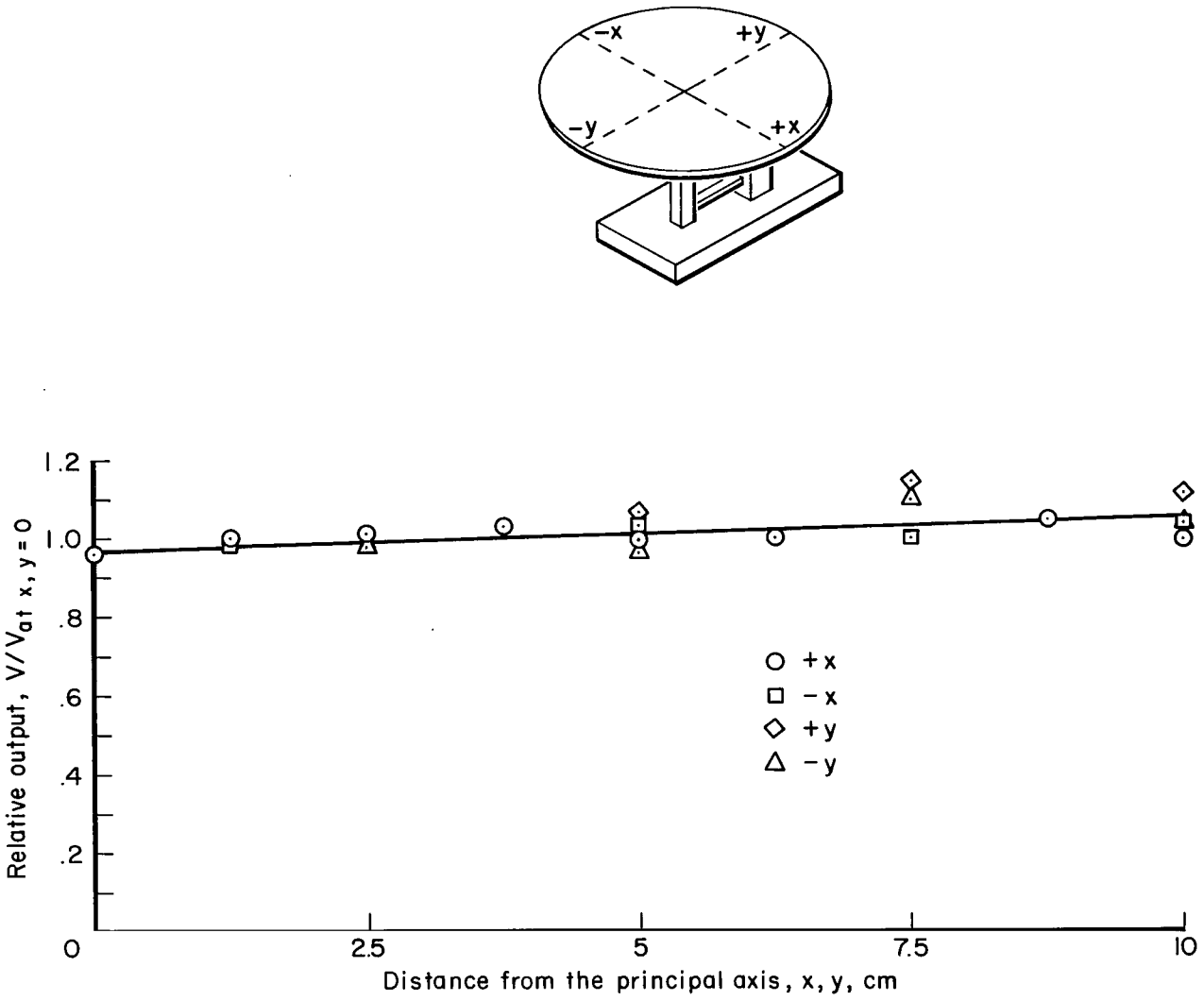

Figure 8.- Transducer response as a function of bead-drop impact location for impacts of constant momentum.

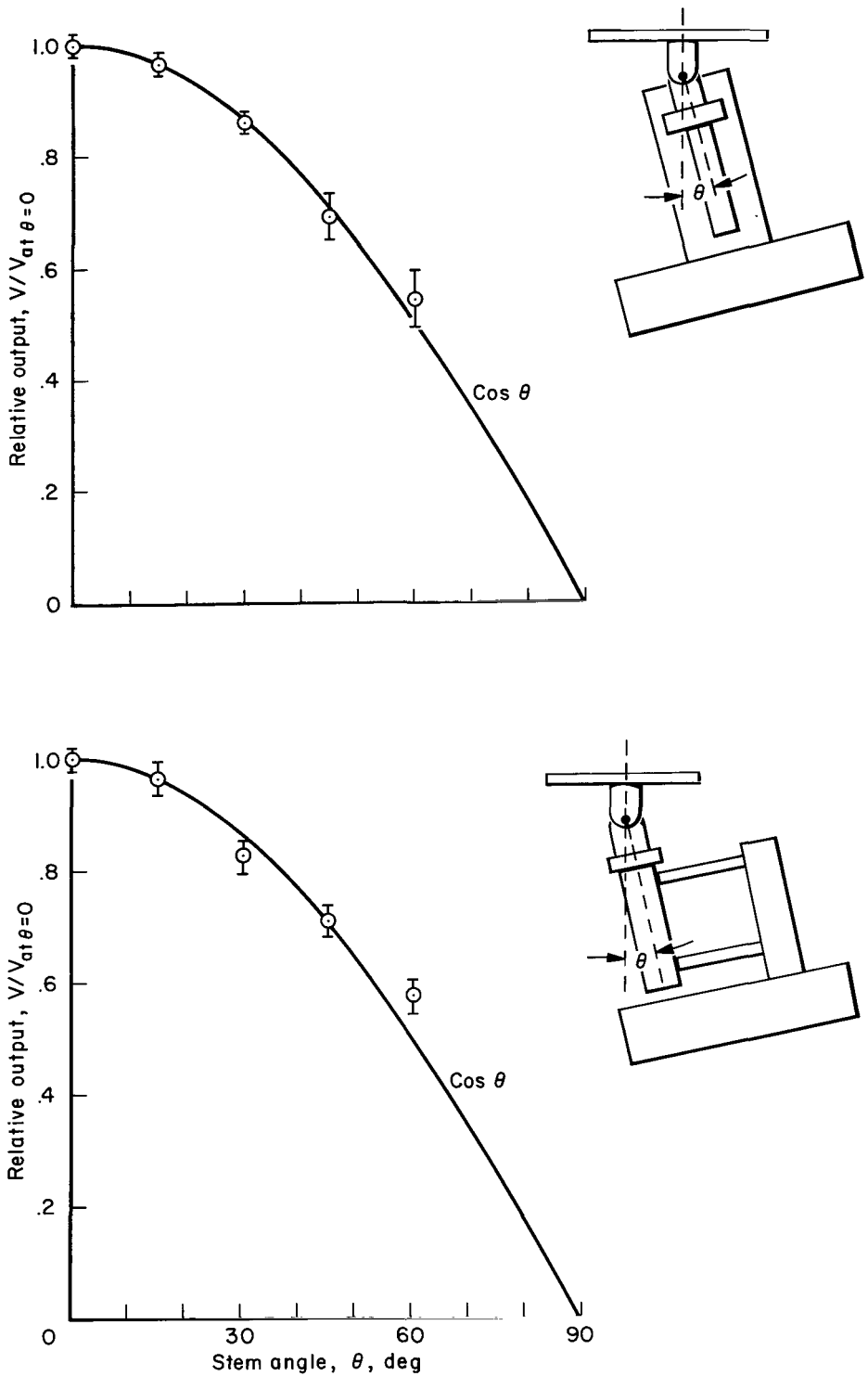

Figure 9.- Transducer response as a function of stem angle relative to impact direction for impacts of constant momentum.

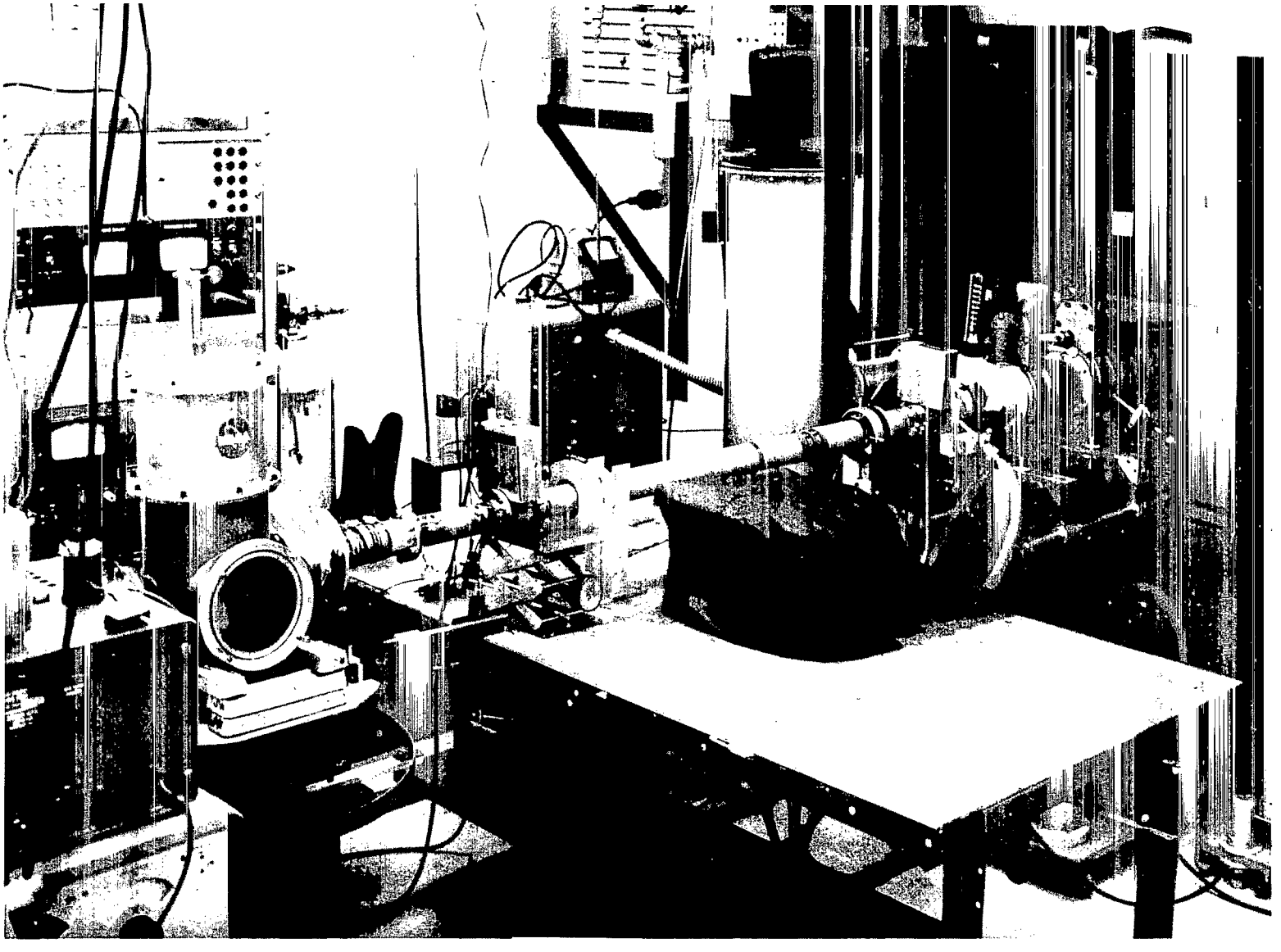

A-31934

Figure 10.- Test apparatus for measuring hypervelocity particle impacts.

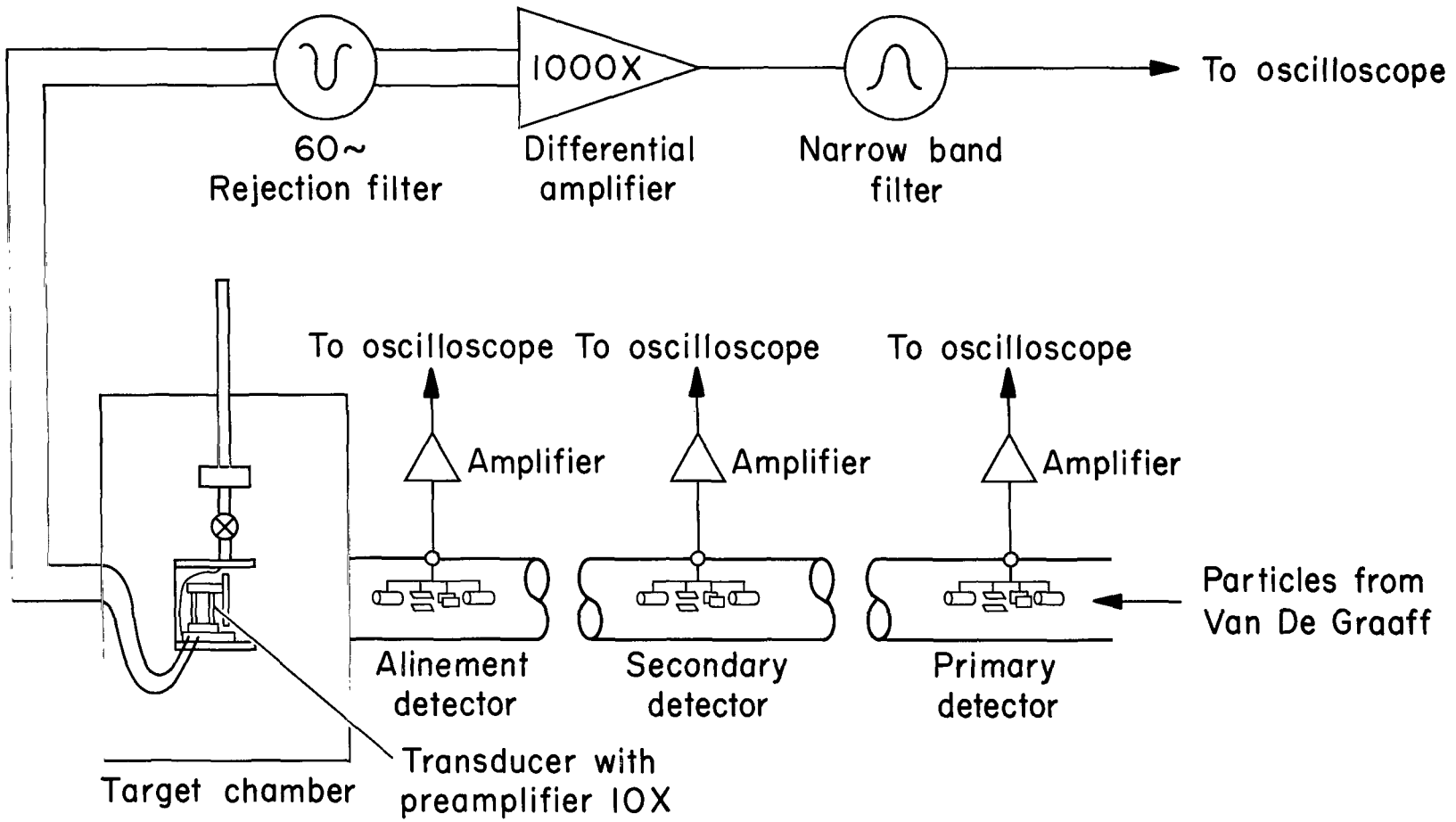

Figure 11.- Schematic diagram of apparatus and instrumentation.

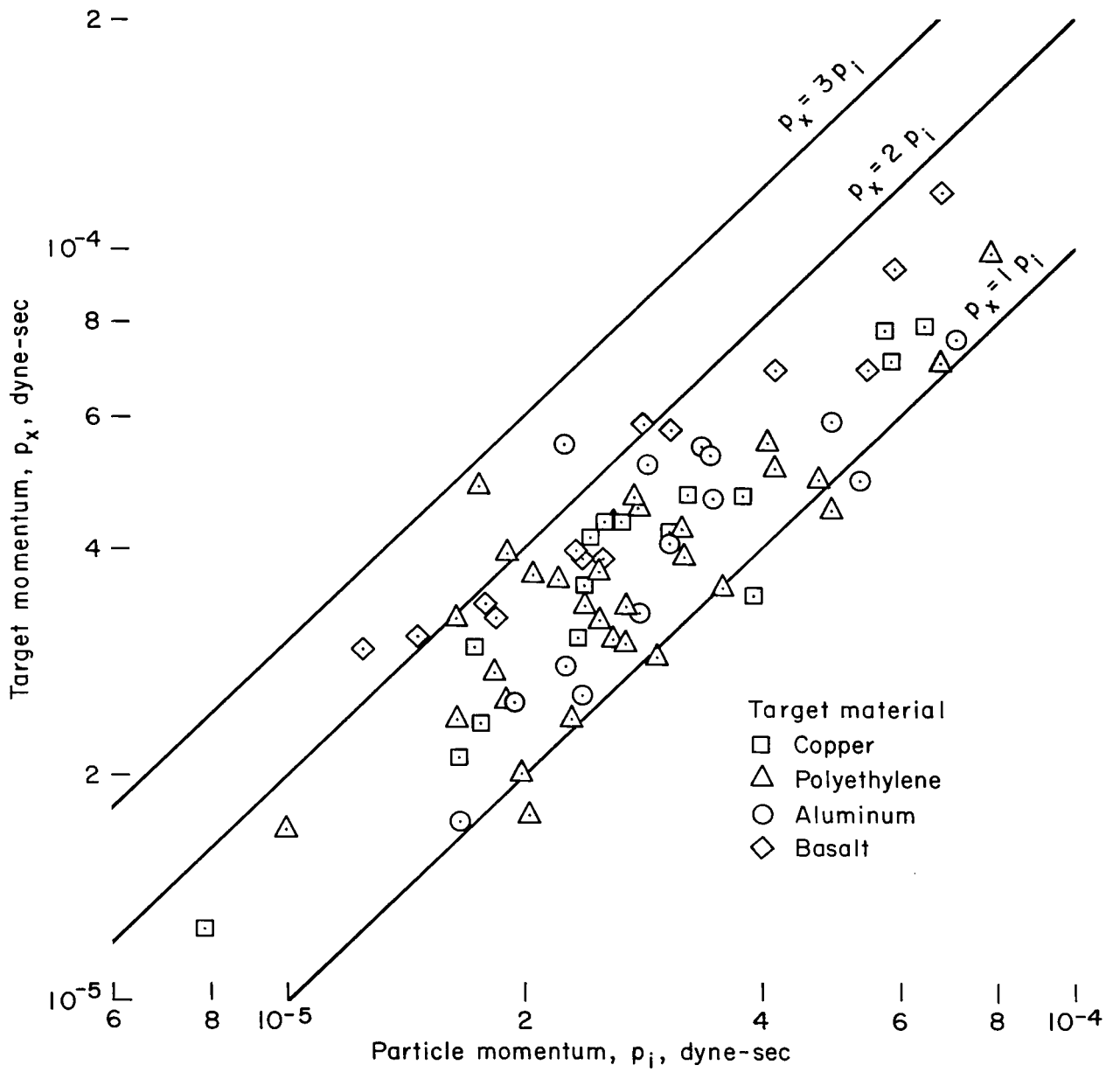

Figure 12.- Target momentum as a function of particle momentun for accelerated iron spheres of 1.6 to 4.5 microns diameter.

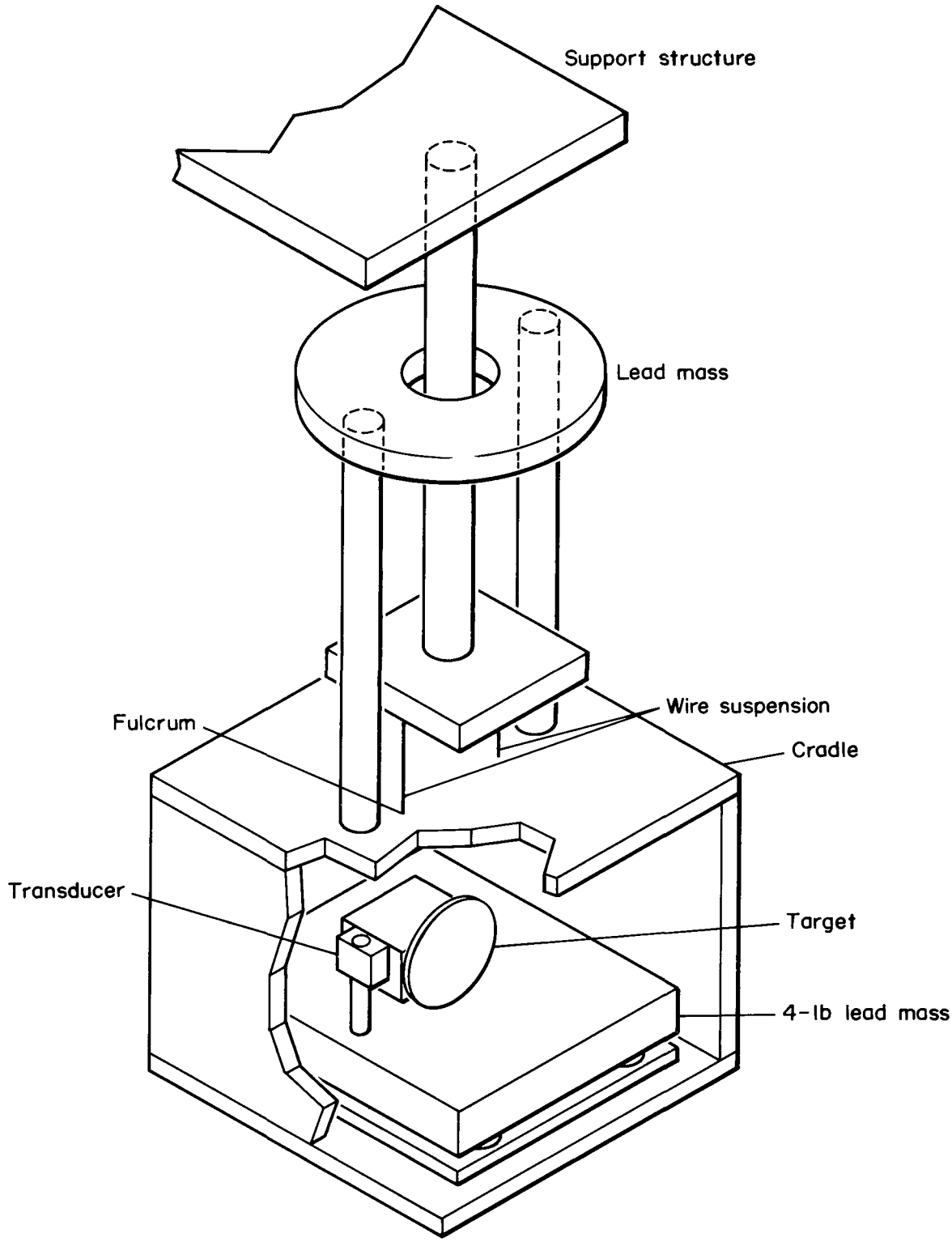

Figure 13.- Transducer suspension arrangement for mechanical noise isolation during hypervelocity tests.

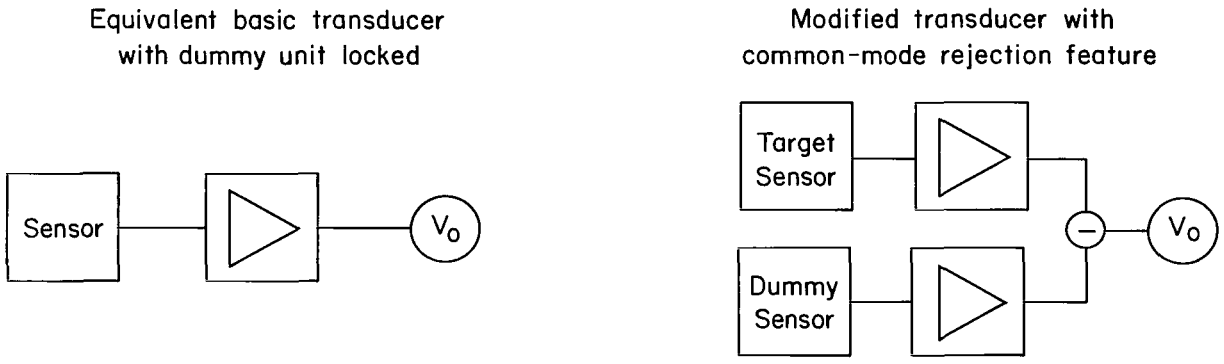

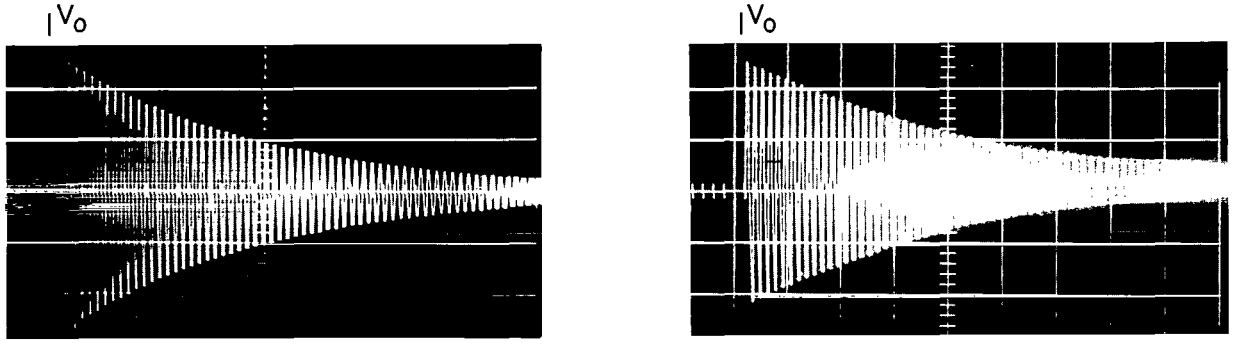

(a) Bead-drop impacts.

(b) Induced wide-band gaussian noise.

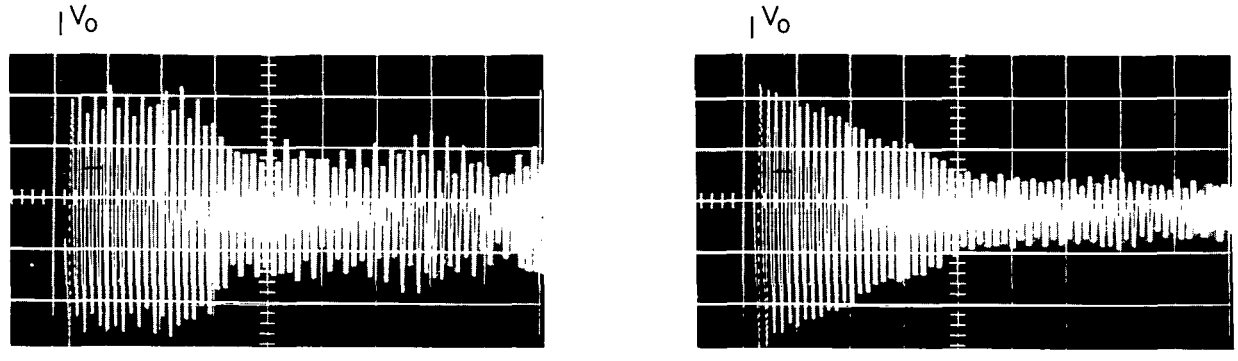

(c) Bead-drop impacts with wide-band gaussian noise.

Figure 14.- Effectiveness of common-mode noise rejection feature for application in an environment of wide-band gaussian noise.

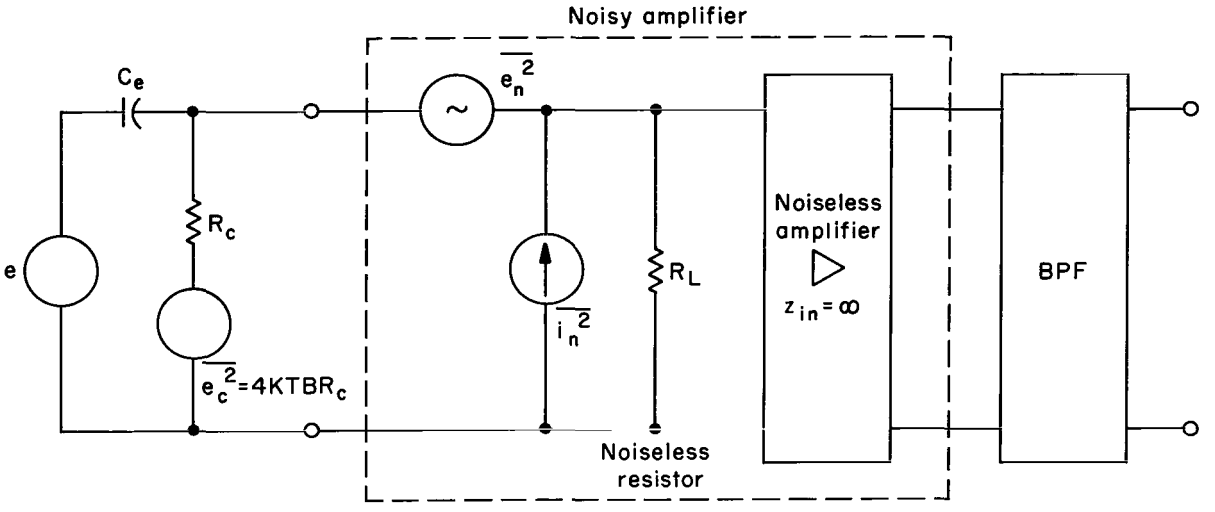

(a) Transducer followed by a noisy amplifier and filter.

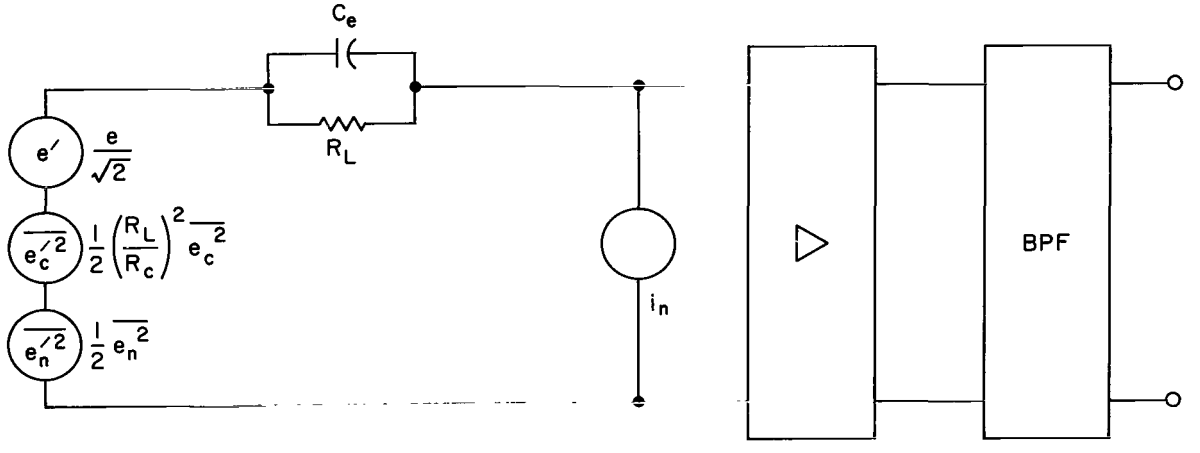

(b) Transducer and amplifier noise sources combined for $R_c \gg R_L$ and $X_e = R_L$.

Figure 15.- Noise sources in the transducer-amplifier combination.

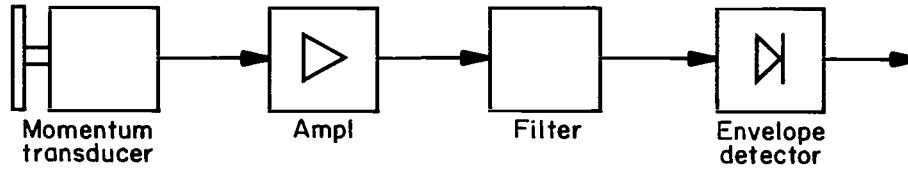

(a) Block diagram of the micrometeoroid momentum measurement system.

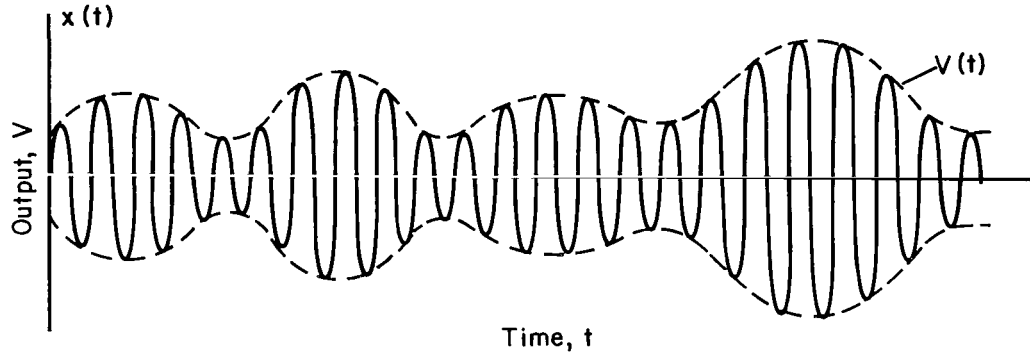

(b) Narrow-band gaussian noise and its envelope.

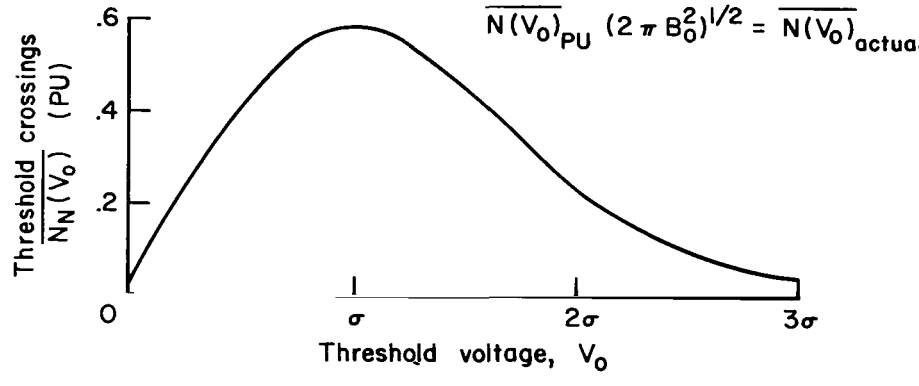

(c) Number of threshold crossings per second as a function of threshold voltage.

Figure 16.- Transducer system noise response as related to filter bandwidth.

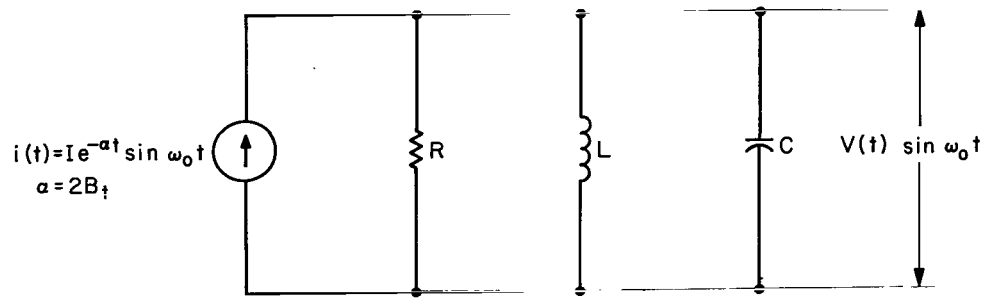

(a) Single tuned band-pass amplifier.

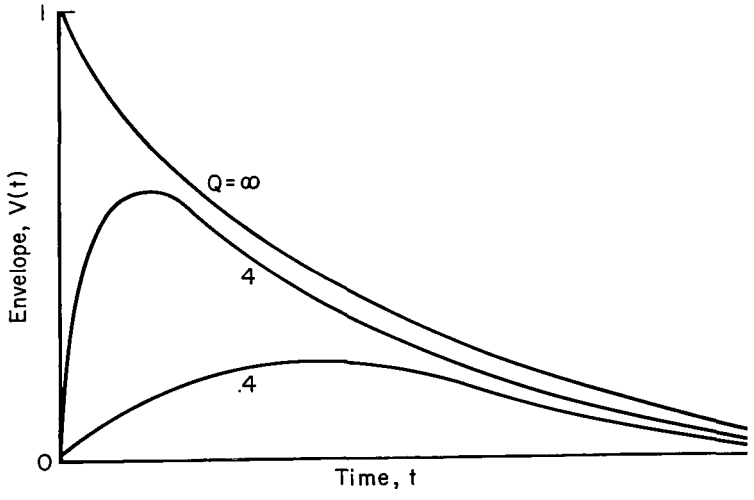

(b) Output envelopes for various filter to transducer bandwidth ratios.

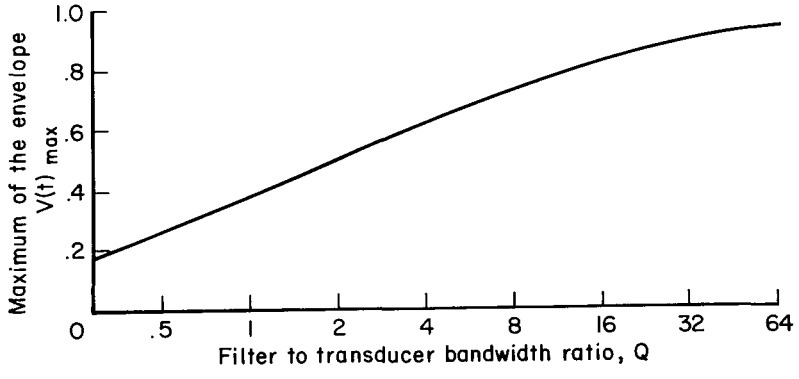

(c) Relative peak amplitude of the envelope as a function of filter bandwidth.

Figure 17.- Transducer system signal response as related to filter bandwidth.

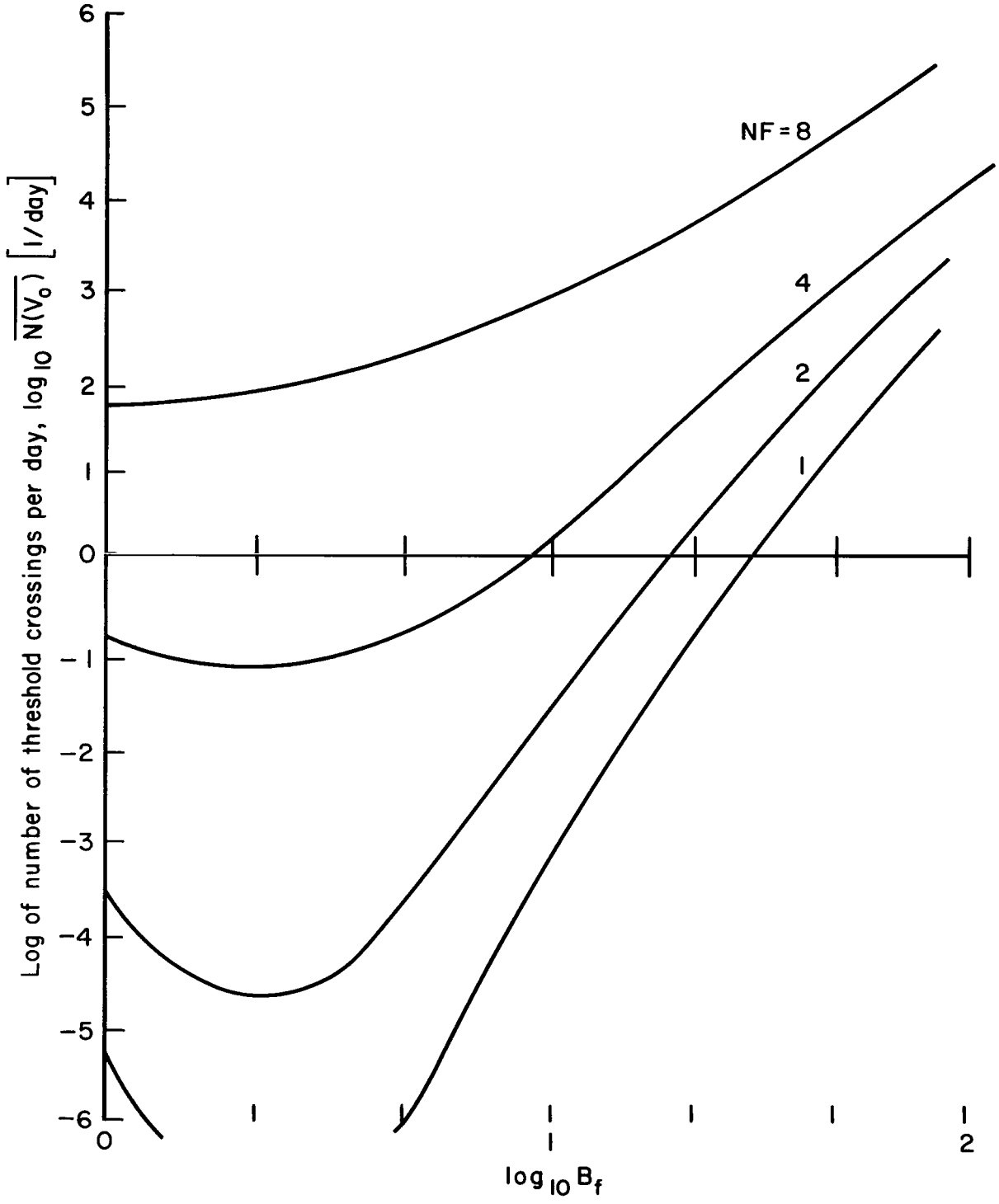

Figure 18.- Number of threshold crossings per day for various noise factors as a function of filter bandwidth for a transducer momentum threshold of 10^{-5} dyne-sec, and a transducer bandwidth of B_t = 2 cps.

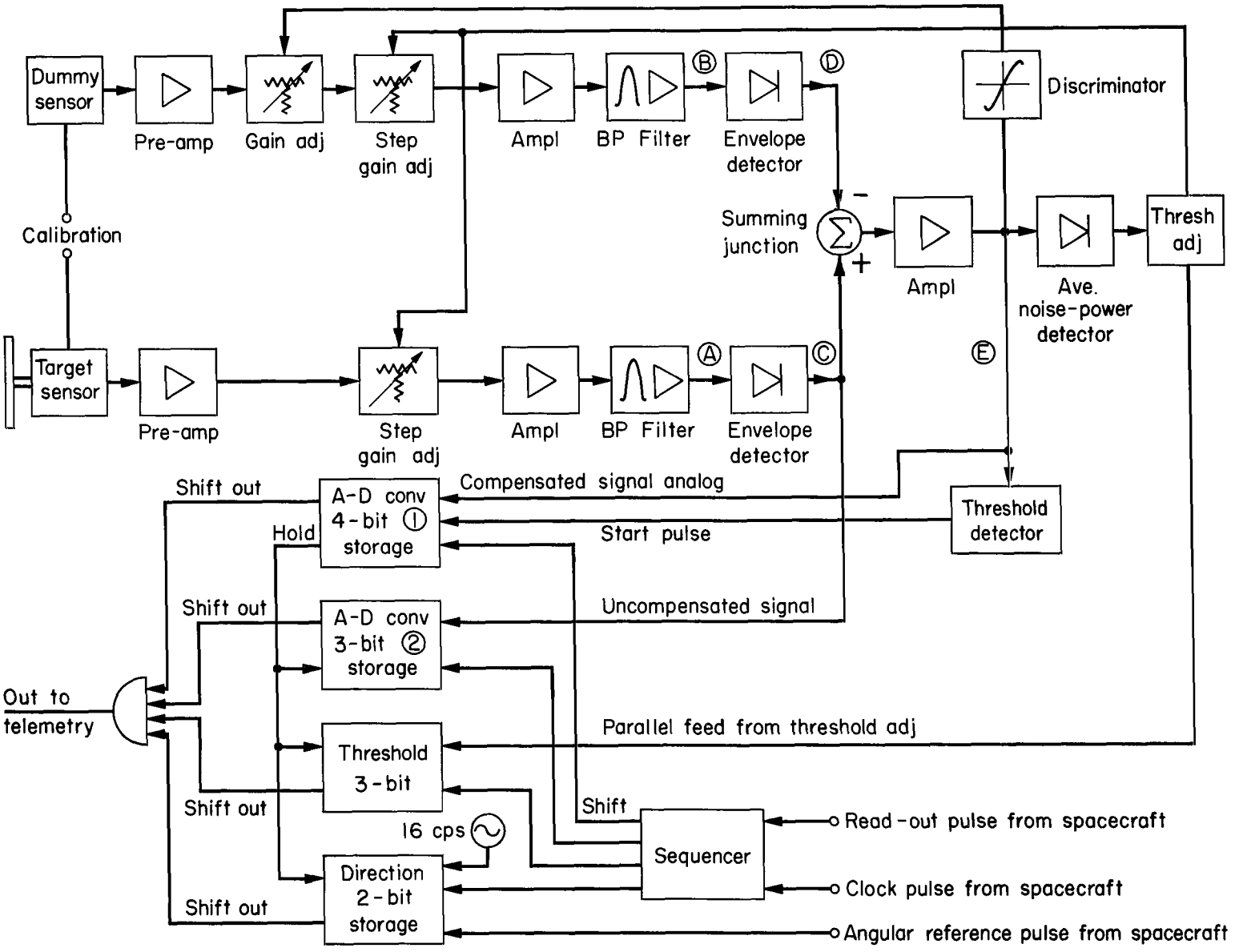

Figure 19.- Block diagram of a micrometeoroid momentum detector system for low data rates.

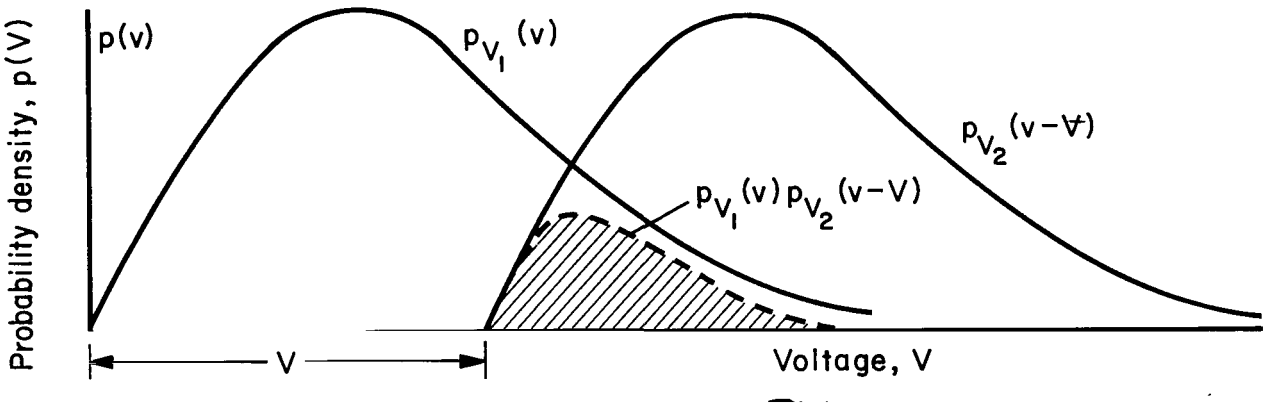

(a) Graphical representation of the calculation of p(V).

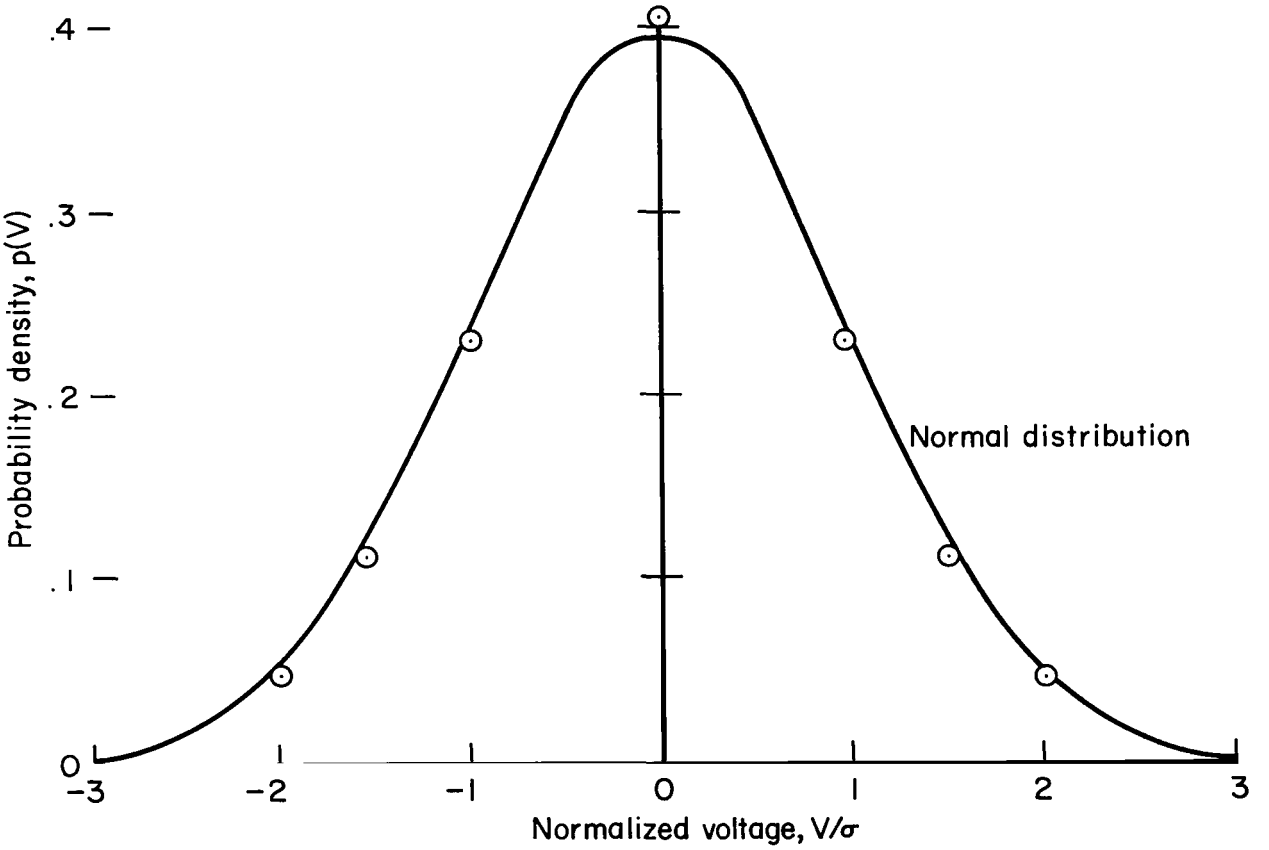

(b) Computed points of p(V) and a normal distribution curve with the same variance.

Figure 20.- Noise statistics of a micrometeoroid momentum detector system.

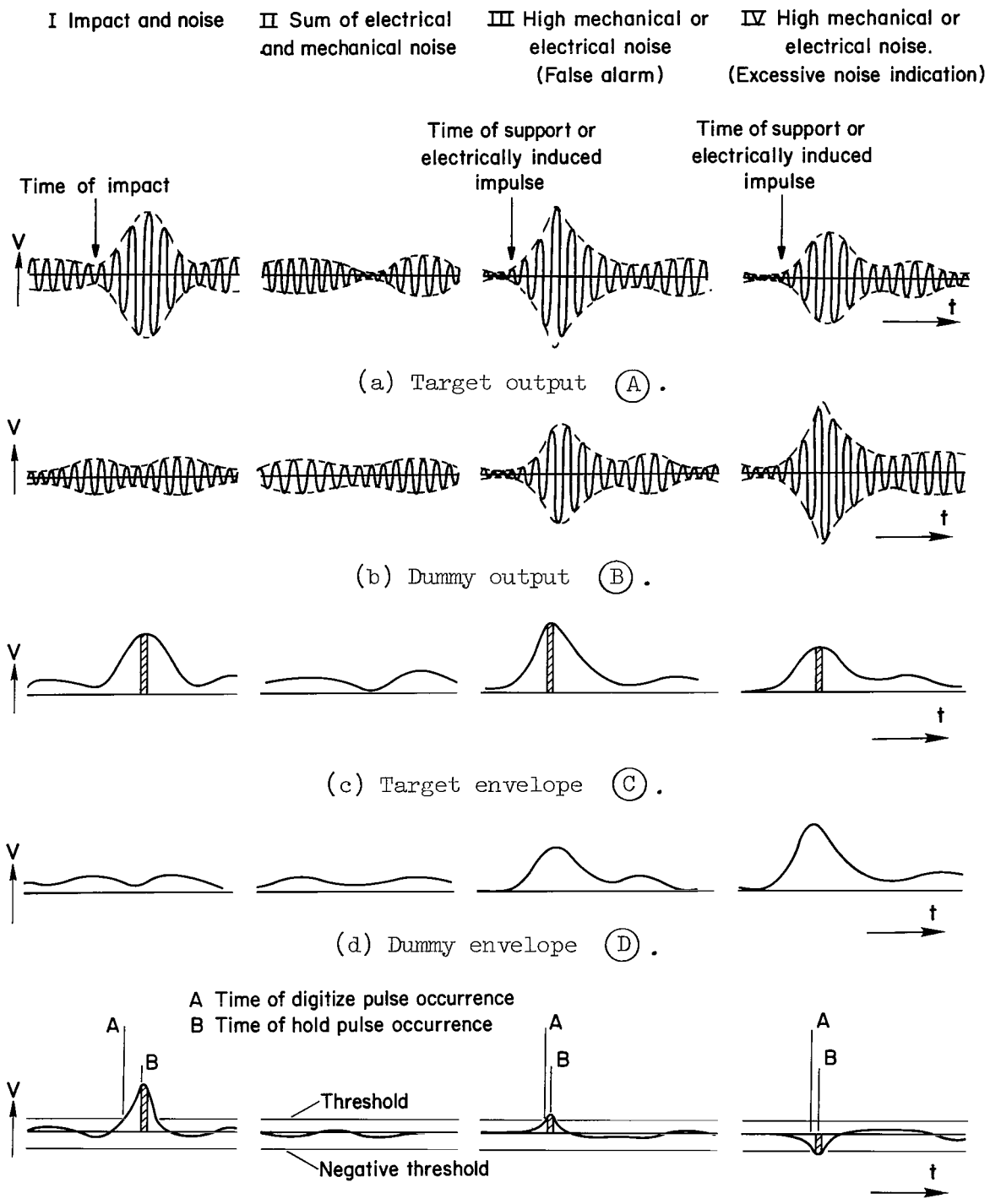

Figure 21.- Signals at various locations of a micrometeoroid momentum detector system. Locations identified by letter designation in figure 19.

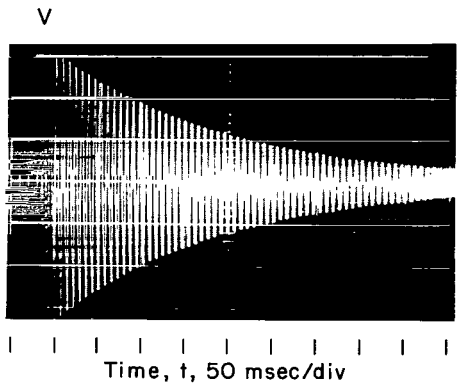

(a) Impulse response.

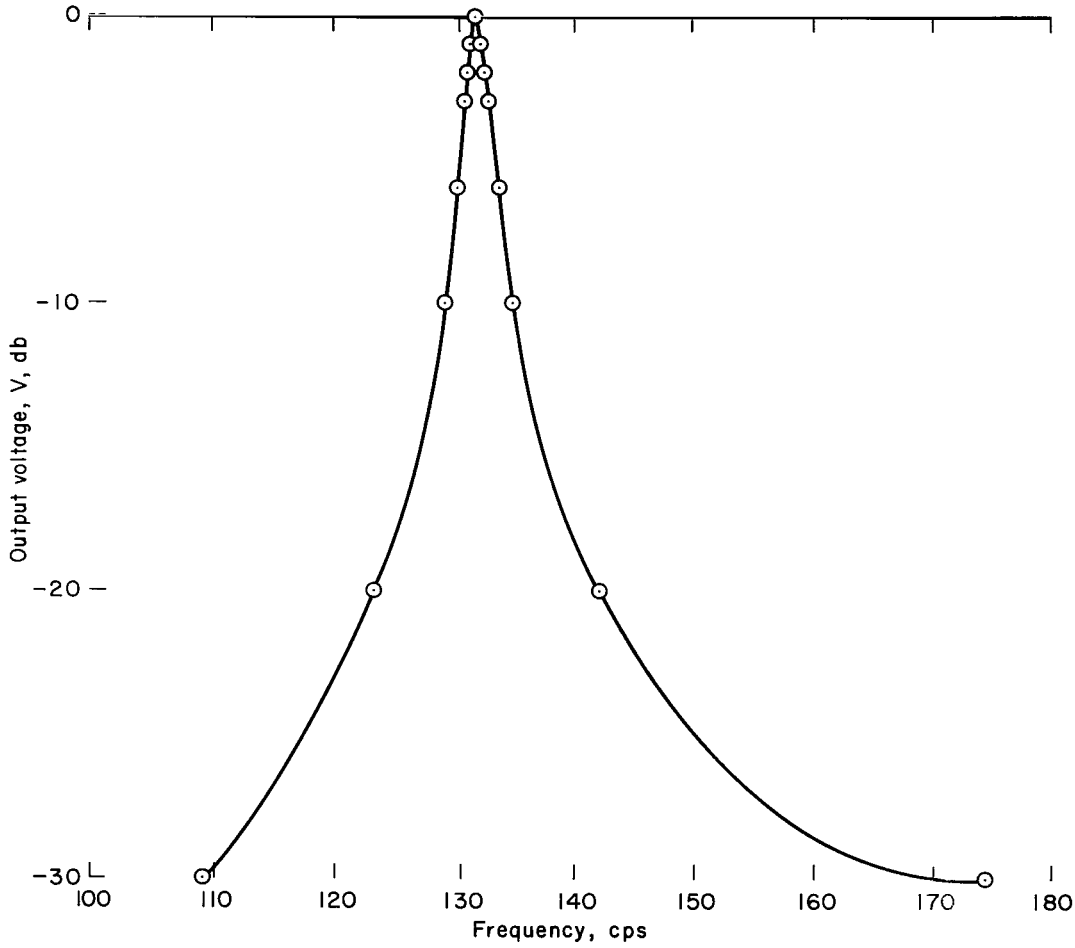

(b) Frequency response.

Figure 22.- Response of the transducer used as an electromechanical filter.

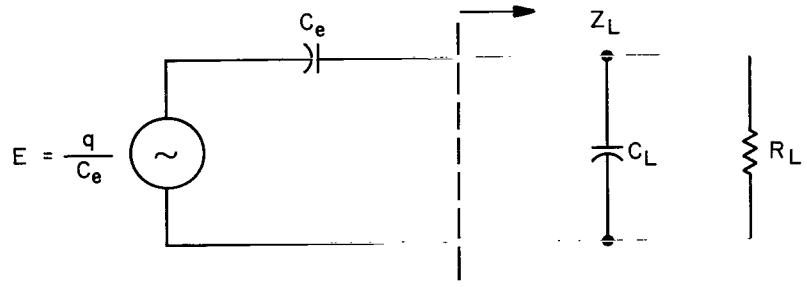

(a) Simplified equivalent electrical circuit of the transducer with load.

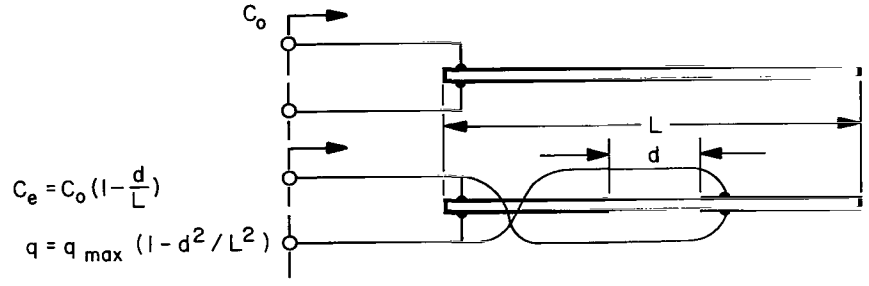

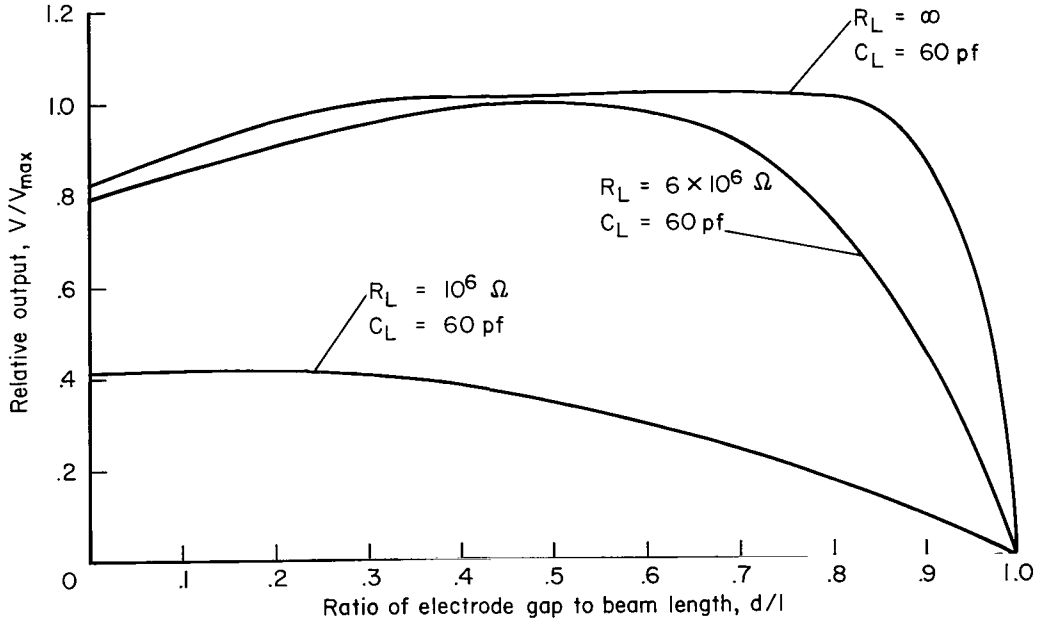

(b) The computed transducer response as a function of the ratio of electrode gap to length for various values of load impedance.

Figure 23.- The effect of beam electrode separation on transducer relative output.

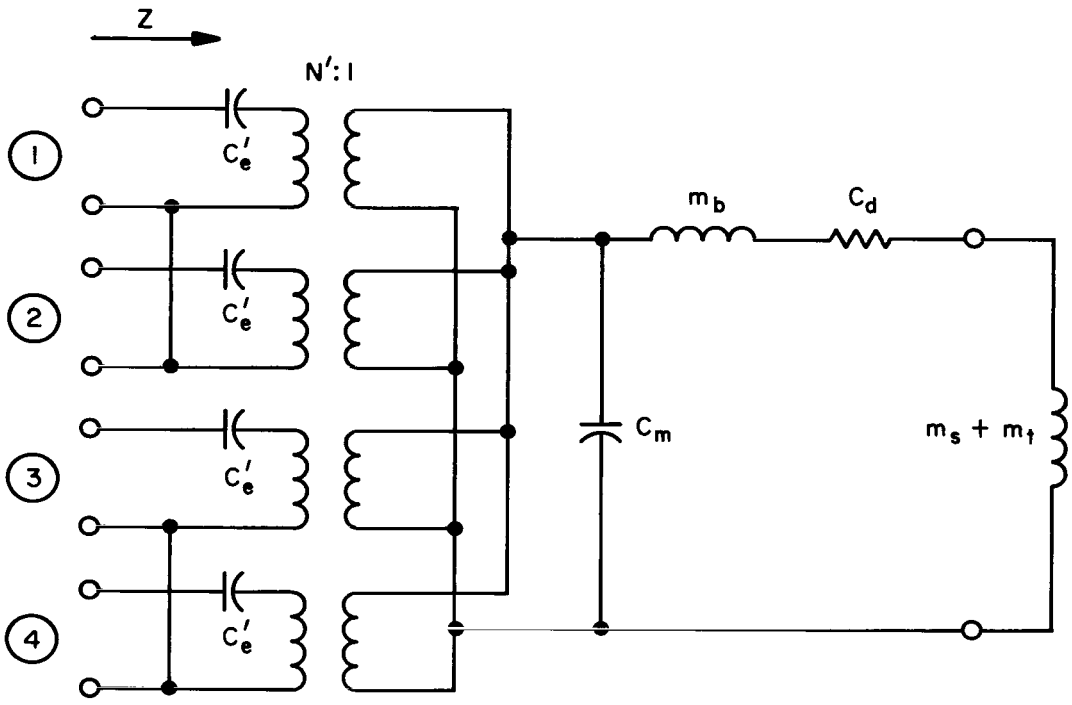

(a) Simplified electromechanical equivalent circuit of the transducer.

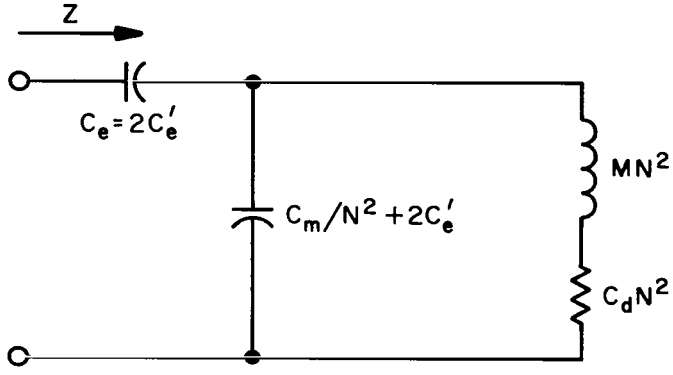

(b) Simplified electrical equivalent circuit of the transducer. Outputs 3 and 4 are short-circuited and outputs 1 and 2 are open.

Figure 24.- Transducer equivalent circuits.

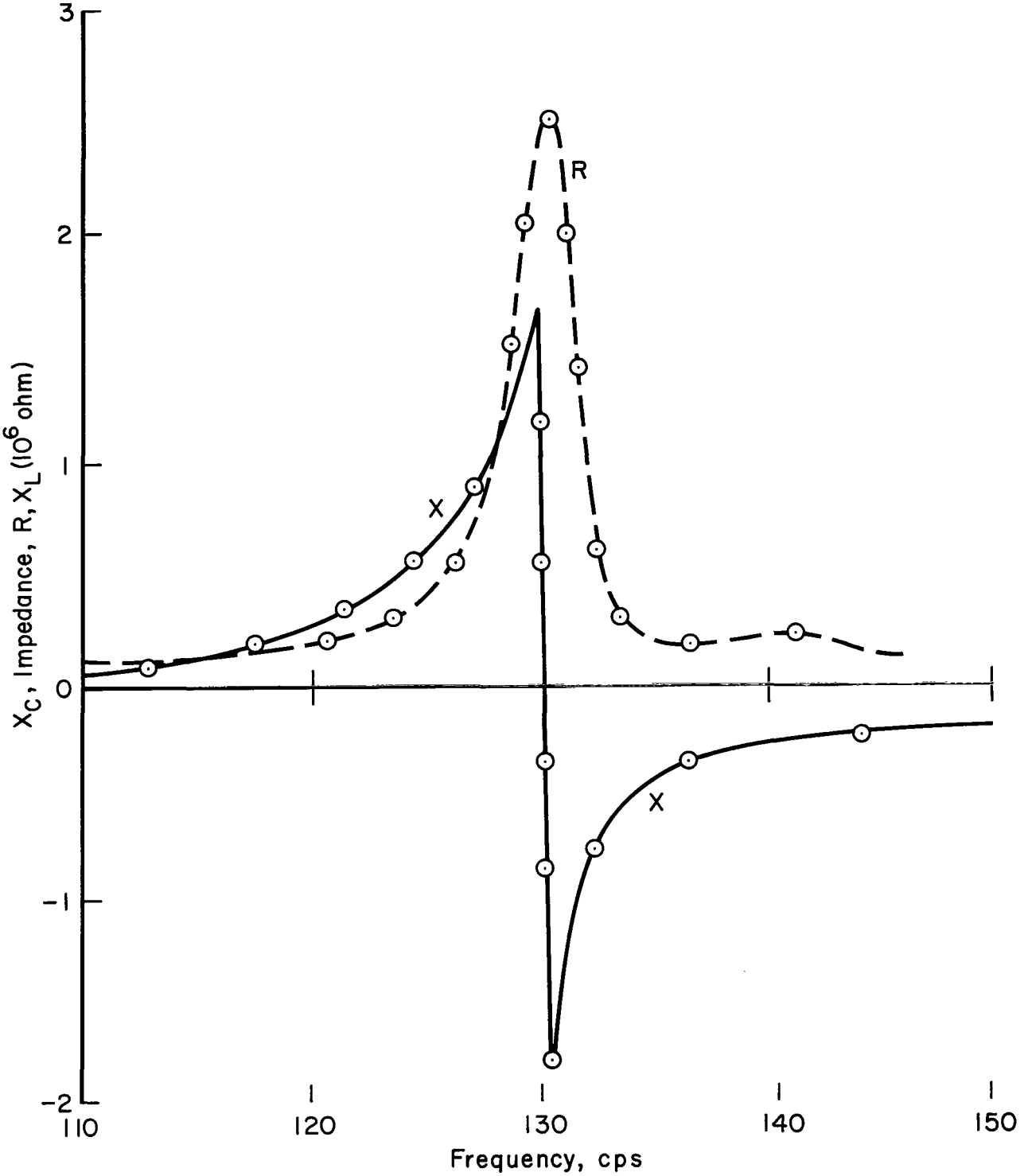

Figure 25.- Measured electrical impedance of the transducer as a function of frequency. Reactance of the series capacitance C_e mathematically subtracted.

NASA-Langley, 1965 A-796

"The aeronautical and space activities of the United States shall be conducted so as to contribute . . . to the expansion of human knowledge of phenomena in the atmosphere and space. The Administration shall provide for the widest practicable and appropriate dissemination of information concerning its activities and the results thereof."

—NATIONAL AERONAUTICS AND SPACE ACT OF 1958

NASA SCIENTIFIC AND TECHNICAL PUBLICATIONS

TECHNICAL REPORTS: Scientific and technical information considered important, complete, and a lasting contribution to existing knowledge.

TECHNICAL NOTES: Information less broad in scope but nevertheless of importance as a contribution to existing knowledge.

TECHNICAL MEMORANDUMS: Information receiving limited distribution because of preliminary data, security classification, or other reasons.

CONTRACTOR REPORTS: Technical information generated in connection with a NASA contract or grant and released under NASA auspices.

TECHNICAL TRANSLATIONS: Information published in a foreign language considered to merit NASA distribution in English.

TECHNICAL REPRINTS: Information derived from NASA activities and initially published in the form of journal articles.

SPECIAL PUBLICATIONS: Information derived from or of value to NASA activities but not necessarily reporting the results of individual NASA-programmed scientific efforts. Publications include conference proceedings, monographs, data compilations, handbooks, sourcebooks, and special bibliographies.

Details on the availability of these publications may be obtained from:

SCIENTIFIC AND TECHNICAL INFORMATION DIVISION

NATIONAL AERONAUTICS AND SPACE ADMINISTRATION

Washington, D.C. 20546